Applied Mathematical Modelling 38 (2014) 5836–5857

Contents lists available at ScienceDirect

Applied Mathematical Modelling

journal homepage: www.elsevier.com/locate/apm

Analysis of numerical stability of algebraic oceanic turbulent mixing layer models

T. Chacón Rebollo [a,*], M. Gómez Mármol [b], S. Rubino [a]

[a] Dpto. de Ecuaciones Diferenciales y Análisis Numérico & IMUS, Universidad de Sevilla, Spain
[b] Dpto. de Ecuaciones Diferenciales y Análisis Numérico, Universidad de Sevilla, Spain

ARTICLE INFO

Article history:
Received 3 May 2013
Received in revised form 9 January 2014
Accepted 23 April 2014
Available online 10 May 2014

Keywords:
Oceanic turbulent mixing layers
Gradient Richardson number
Eddy diffusion models
Primitive Equations of the ocean

ABSTRACT

In this paper, we study the stability of oceanic turbulent mixing layers by the finite element method with respect to perturbations of the data. We prove that the equilibria states depend continuously on the data, and that they are asymptotically stable in time, when approximated by standard numerical schemes. We also perform some numerical tests for realistic initial conditions, that also show that the mixing-layer configurations are stable under perturbations of the data, in addition to confirm the theoretical expectations of our analysis.

1. Introduction

The oceanic flow and the global climate is largely influenced by the dynamics of the oceanic mixing layers. Indeed, due to the larger specific heat of the water, the top 2.5 m depth oceanic layer contains as much heat as the full atmosphere over it. In addition, the heat stored within the oceanic mixing layer provides a source for heat that drives global variability such as El Niño. We address in this paper the numerical modeling of the oceanic mixing layer, by means of algebraic turbulence models based upon vertical turbulent diffusion. The formation of the mixing layer is due to the surface shear induced by the winds, that generates a strong turbulent mixing dominated by vertical fluxes. In global oceanic circulation the mixed layer plays an important role, because it determines how momentum, heat and eventually freshwater are entering or leaving the ocean. The numerical models of global oceanic circulation include specific models of mixing layers, in particular the algebraic ones, in order to better take into account the influence of these surface interactions (Cf. [1,2]).

We consider here the algebraic turbulent mixing-layer models, introduced in the 80's by Pacanowski–Philander (Cf. [3]). These models apply to stratified shear flow, that is assumed to have reached a vertical equilibrium, after the vertical mixing generated by the wind stress has been re-stabilized by buoyancy forces. Thus, only vertical eddy diffusion effects are included, and the vertical velocity is assumed to vanish. These simplifications lead to the following model:

$$\begin{cases} \partial_t u - \partial_z(\nu_1 \partial_z u) = 0, \\ \partial_t v - \partial_z(\nu_1 \partial_z v) = 0, \quad \text{for } t \geqslant 0 \text{ and } -h \leqslant z \leqslant 0, \\ \partial_t \rho - \partial_z(\nu_2 \partial_z \rho) = 0, \end{cases} \tag{1}$$

* Corresponding author. Tel.: +34 954557989.
E-mail addresses: chacon@us.es (T. Chacón Rebollo), macarena@us.es (M. Gómez Mármol), samuele@us.es (S. Rubino).

http://dx.doi.org/10.1016/j.apm.2014.04.050
0307-904X/

where (u, v) is the horizontal velocity and ρ is the density, which is considered as a thermodynamic variable, as it depends on temperature and salinity through a state law. Also, the symbols ν_1 and ν_2 respectively stand for the total viscosity and diffusion, yield by $\nu_1 = a_1 + \nu_{T1},\ \nu_2 = a_2 + \nu_{T2}$ where a_1 and a_2 respectively are the laminar viscosity and diffusion coefficients, and ν_{T1} and ν_{T2} respectively are the eddy viscosity and diffusion coefficients. These are assumed to be functions of the gradient Richardson number R, defined as:

$$R = -\frac{g}{\rho_r}\frac{\partial_z \rho}{(\partial_z u)^2 + (\partial_z v)^2}, \tag{2}$$

where g is the gravity constant and ρ_r is a reference density for the sea water. The Richardson number measures the ratio between stabilizing buoyancy forces and de-stabilizing shear forces. The diffusion coefficients corresponding to the original Pacanowski–Philander (PP) model (Cf. [3]) are given by:

$$\nu_1 = f_1(R), \quad \nu_2 = f_2(R),$$

where:

$$f_1(R) = a_1 + \frac{b_1}{(1+5R)^2}, \quad f_2(R) = a_2 + \frac{f_1(R)}{1+5R}, \quad \text{with } a_1 = 10^{-4},\ b_1 = 10^{-2},\ a_2 = 10^{-5}. \tag{3}$$

The Gent (Cf. [4]) model is just a variant of the PP model, designed to better fit experimental data, given by:

$$f_1(R) = a_1 + \frac{b_1}{(1+10R)^2}, \quad f_2(R) = a_2 + \frac{b_1}{(1+10R)^3}, \quad \text{with } b_1 = 10^{-1}. \tag{4}$$

The PP and Gent models become numerically unstable if the initial conditions are physically unstable configurations, corresponding to $R < 0$. In [5] a modeling of the eddy diffusion that remains numerically stable for a certain range of negative gradient Richardson numbers R was introduced:

$$f_1(R) = a_1 + \frac{b_1}{(1+5R)^2}, \quad f_2(R) = a_2 + \frac{f_1(R)}{(1+5R)^2}, \tag{5}$$

with the same constants of the PP model. All these models generate mixing layer profiles in characteristic time scales of the order of several days and linear velocity and density steady profiles in characteristic time scales of the order of one year (Cf. [5]).

In practice, mixing-layer models are coupled with 3D models of global circulation, that yield the boundary values for velocity and density at the bottom of the layer. This allows to use finer grids (in the vertical direction) to compute the heat exchange through the ocean surface. This is the case for instance of the finite element FESOM model (Cf. [2]). More complex parameterizations of the vertical turbulent mixing, like the k–ε model, are also used, for instance in the finite-difference GOTM model (Cf. [1]). However, the analysis of these models is technically much more difficult and, up to the knowledge of the authors, there are no references addressing them at the present date.

We shall consider the following initial and boundary conditions for model (1):

$$\begin{cases} \nu_1 \partial_z u = Q_u,\ \nu_1 \partial_z v = Q_v,\ \nu_2 \partial_z \rho = Q_\rho & \text{at the surface } z = 0, \\ u = u_b,\ v = v_b,\ \rho = \rho_b & \text{at the depth } z = -h, \\ u = u_0,\ v = v_0,\ \rho = \rho_0 & \text{at initial time } t = 0, \end{cases} \tag{6}$$

where the plane $z = -h$ is located below the mixing layer. The Neumann boundary conditions at the surface represent the fluxes at the sea–surface that model the forcing by the atmosphere. In particular: $Q_u,\ Q_v$ are the surface momentum fluxes and Q_ρ represents thermodynamic fluxes. The momentum fluxes are given by $Q_u = (\rho_a/\rho_r)V_u,\ Q_v = (\rho_a/\rho_r)V_v$, where ρ_a is the air density, ρ_r is a reference density, and V_u and V_v are respectively the stresses exerted by the zonal and the meridional winds, given by:

$$(V_u, V_v) = C_D \left|\mathbf{U}^a\right| \mathbf{U}^a,$$

where $\mathbf{U}^a = (u_a, v_a)$ is the air velocity at the atmospheric boundary layer, and $C_D\,(= 1.2 \cdot 10^{-3})$ is a friction coefficient (Cf. [6]). Note that, in practice, all the data depend on the horizontal variables (x, y), although for brevity we shall not explicit them.

A linear analysis of asymptotic stability of continuous equilibria of model (1)–(6) has been performed in Bennis et al. [5], in addition to a numerical investigation of its approximation by standard finite element approximations.

In the present paper, we perform a non-linear stability analysis of algebraic turbulence models for oceanic mixing-layers. We study on one side the asymptotic stability of perturbed models. We prove that the perturbed equilibria are unique and are asymptotically reached by time iterates of standard finite element discretizations. This analysis applies to negative surface thermodynamic fluxes, and is complemented with some numerical tests that show that the steady states for density are rather insensitive to perturbations, while those for zonal and meridional velocities are largely sensitive.

We also perform a numerical investigation of the finite-time stability. By comparing with the solutions of a 2D model of Primitive Equations of the ocean, we show that the 1D model provide mixing-layer profiles on time scales of the order of two

days, which are accurate with respect to 2D perturbations of the initial conditions, and with respect to horizontal pressure gradients.

As a conclusion, we obtain that algebraic turbulence models for oceanic mixing-layers bear excellent stability properties and provide good predictions of the formation of mixing-layer profiles and of flow equilibria, even under perturbations of the data.

The paper is structured as follows: In Section 2, we analyze the equilibria of the perturbed model. Section 3 introduces the numerical discretization of the mixing-layer model, which is analyzed in Section 4. This analysis deals with existence and uniqueness of discrete steady states, and the analysis of asymptotic convergence of the discrete time iterates to the continuous equilibria. Some numerical tests confirm the theoretical predictions. In Section 5 we perform the numerical investigation of the finite-time stability of the mixing-layer model with respect to 2D perturbations. Finally in Section 6 we summarize the main conclusions of our study.

2. Equilibria states of perturbed model

We prove in this section that there exist steady solutions of model (1)–(6) for slightly perturbed data. These perturbations may correspond to errors in the experimental measurements, roundoff computational errors, errors in the boundary data coming from the approximate solution of the 3D global model, etc. The steady solutions correspond to an equilibrium between de-stabilizing wind shear effects and stabilizing surface thermodynamic fluxes.

Let us consider the perturbed model:

$$\begin{cases} \partial_t u - \partial_z(\nu_1 \partial_z u) = D_u, \\ \partial_t v - \partial_z(\nu_1 \partial_z v) = D_v, \quad \text{for } t \geqslant 0 \text{ and } -h \leqslant z \leqslant 0, \\ \partial_t \rho - \partial_z(\nu_2 \partial_z \rho) = D_\rho, \end{cases} \tag{7}$$

with the perturbed boundary and initial conditions:

$$\begin{cases} \nu_1 \partial_z u = \sigma_u, \ \nu_1 \partial_z v = \sigma_v, \ \nu_2 \partial_z \rho = \sigma_\rho \quad \text{at the surface } z = 0, \\ u = U_b, \ v = V_b, \ \rho = R_b \quad \text{at the depth } z = -h, \\ u = U_0, \ v = V_0, \ \rho = R_0 \quad \text{at initial time } t = 0, \end{cases} \tag{8}$$

where D_u, D_v and D_ρ are functions of z and σ_u, σ_v, σ_ρ, U_b, V_b and R_b are constants. Let us denote $I = (-h, 0)$, and define the functions:

$$d_u(z) = \int_z^0 D_u(s)\, ds, \quad d_v(z) = \int_z^0 D_v(s)\, ds, \quad d_\rho(z) = \int_z^0 D_\rho(s)\, ds.$$

The existence and uniqueness of equilibria for this problem are given by the following:

Theorem 2.1. *Assume that for any $z \in I$ the implicit algebraic equation:*

$$R = G(z) \frac{[f_1(R)]^2}{f_2(R)}, \tag{9}$$

where $G(z)$ is the function defined by:

$$G(z) = -\frac{g}{\rho_r} \frac{d_\rho(z) + \sigma_\rho}{(d_u(z) + \sigma_u)^2 + (d_v(z) + \sigma_v)^2}, \tag{10}$$

admits at least a solution R^e. Then, to each solution R^e there exists a unique associated equilibrium solution of problem (7,8) in $[H^1(I)]^3$, given by:

$$\begin{cases} u^e(z) = U_b + \Psi_u(z), \\ v^e(z) = V_b + \Psi_v(z), \\ \rho^e(z) = R_b + \Psi_\rho(z), \end{cases} \tag{11}$$

where:

$$\Psi_u(z) = \int_{-h}^z \frac{d_u(s) + \sigma_u}{f_1(R^e(s))} ds, \quad \Psi_v(z) = \int_{-h}^z \frac{d_v(s) + \sigma_v}{f_1(R^e(s))} ds, \quad \Psi_\rho(z) = \int_{-h}^z \frac{d_\rho(s) + \sigma_\rho}{f_2(R^e(s))} ds. \tag{12}$$

Proof. The equilibrium states of (7) are solutions of the system:

$$\begin{cases} -\partial_z(f_1(R)\partial_z u) = D_u, \\ -\partial_z(f_1(R)\partial_z v) = D_v, \\ -\partial_z(f_2(R)\partial_z \rho) = D_\rho. \end{cases} \tag{13}$$

Integrating the three equations in (13) with respect to z, we obtain:

$$\begin{cases} \partial_z u = (d_u(z) + \sigma_u)/f_1(R), \\ \partial_z v = (d_v(z) + \sigma_v)/f_1(R), \\ \partial_z \rho = (d_\rho(z) + \sigma_\rho)/f_2(R). \end{cases} \tag{14}$$

From (2), we deduce that the equilibrium profiles R^e satisfy the implicit algebraic Eq. (9), and then are functions of z. By integrating with respect to z the three equations in (14), we deduce that the equilibrium solutions of problem (7,8) are given by (11).

To prove the uniqueness of these solutions in $[H^1(I)]^3$, assume that (u_1^e, v_1^e, ρ_1^e) is another equilibrium of problem (7, 8) belonging to $[H^1(I)]^3$. Then, the difference in the first component of the velocity $\delta u = u^e - u_1^e$ weakly satisfies:

$$\partial_z(f_1(R^e)\partial_z \delta u) = 0, \quad v_1 \partial_z \delta u = 0 \quad \text{at} \quad z = 0, \quad \text{and} \quad \delta u = 0 \quad \text{at} \quad z = -h.$$

That is:

$$\int_{-h}^{0} f_1(R^e)\partial_z \delta u \partial_z w = 0, \quad \forall w \in H^1(I) \quad \text{such that} \quad w(-h) = 0.$$

As $f_1(R) \geqslant a_1 > 0$, then $\delta u = 0$. This implies $u^e = u_1^e$. Similarly, we deduce $v^e = v_1^e,\ \rho^e = \rho_1^e$. □

The existence of solutions of the algebraic Eq. (9) is ensured under the following hypothesis:

Hypothesis 1. The fluxes satisfy $Q_u > 0,\ Q_v > 0,\ Q_\rho < 0$ and for some $\lambda \in (0,1)$ it holds:

$$\sigma_u \in (\lambda Q_u, (2-\lambda) Q_u), \quad \sigma_v \in (\lambda Q_v, (2-\lambda) Q_v), \quad \sigma_\rho \in ((2-\lambda) Q_\rho, \lambda Q_\rho), \tag{15}$$

$$\|D_u\|_{L^1(I)} < \frac{\lambda}{2} Q_u, \quad \|D_v\|_{L^1(I)} < \frac{\lambda}{2} Q_v, \quad \|D_\rho\|_{L^1(I)} < \frac{\lambda}{2} |Q_\rho|. \tag{16}$$

The assumption $Q_u > 0,\ Q_v > 0$ means that the wind velocity acts as an un-stabilizing agent for the mixing layer flow, while $Q_\rho < 0$ means that the thermodynamic flux plays a stabilizing role. The conditions (15) and (16) mean that we are considering small perturbations of those data and also of the r.h.s. of Eq. (1). We conclude that for all considered models, there exist steady solutions of problem (1)–(6) that correspond to equilibria between these two effects, for slightly perturbed data:

Corollary 2.1. *Assume that Hypothesis 1 holds. Then the algebraic Eq. (9) admits at least a solution for the PP (3), Gent (4) and Bennis et al. (5) models. As a consequence, to each solution of Eq. (9) there corresponds a unique equilibrium solution of (7,8) given by (11).*

Proof. The solutions of the implicit algebraic Eq. (9) may be interpreted as the intersection of the curves:

$$h_z(R) = \frac{1}{G(z)} R, \quad k(R) = \frac{[f_1(R)]^2}{f_2(R)}.$$

For the Bennis et al. model (5), there exists a unique gradient Richardson number R^e whenever $G(z) > 0$, as this implies that the slope of the straight h_z is positive (see Fig. 1). For the PP (3) and Gent (4) models, if $G(z) > 0$ there exist two solutions of Eq. (9) (see Figs. 2 and 3). Hypothesis 1 implies that $G(z) > 0$ for all $z \in [-h, 0]$. □

Remark 2.1. The equilibria of the un-perturbed model (1) is studied in [5]. In that case, R^e does not depend on z, and, as consequence, the equilibrium profiles for velocity and density are linear. The equilibria for the perturbed model (7,8) provided by Theorem 2.1 converge to those of the un-perturbed model as the perturbations in the data vanish. This readily follows from identities (9)–(12).

3. Numerical discretization of the 1D model

In this section we discretize the initial-boundary value problem (7,8) by linear piecewise finite elements. To describe these schemes, assume that the interval $\bar{I} = [-h, 0]$ is divided into N subintervals of length $\Delta z = h/N$, with nodes $z_i = -h + i\Delta z,\ i = 0, \ldots, N$, and construct the finite element space:

$$V_\Delta = \{ w_\Delta \in C^0(\bar{I}) \,|\, w_{\Delta|_{(z_{i-1}, z_i)}} \text{ is affine, } i = 1, \ldots, N;\ w_\Delta(-h) = 0 \}. \tag{17}$$

To discretize the equation for u, for instance, we consider on one hand the semi-implicit method:

Obtain $u_\Delta \in U_b + V_\Delta$ such that

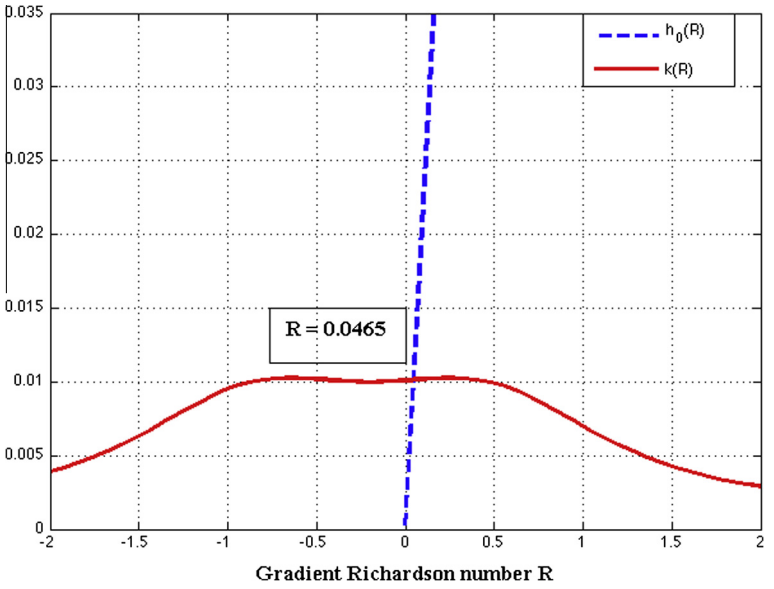

Fig. 1. Solution of the equation for equilibrium gradient Richardson number with model (5).

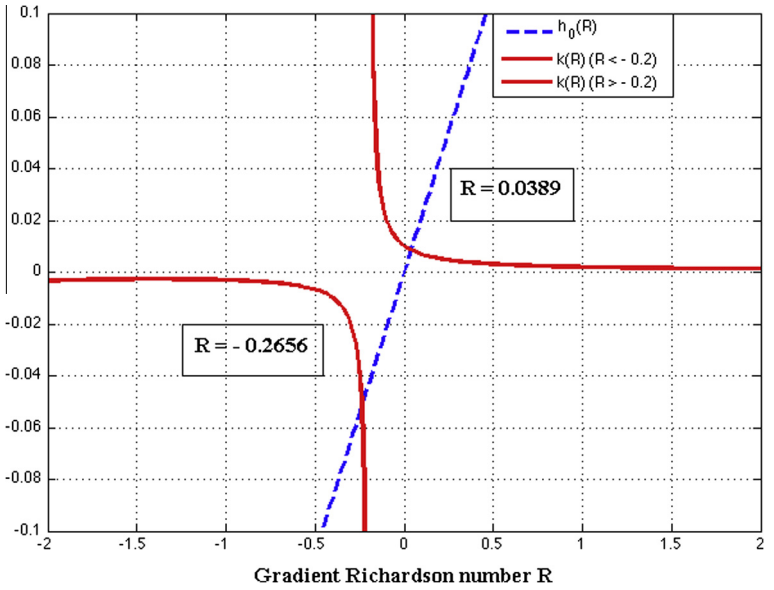

Fig. 2. Solution of the equation for equilibrium gradient Richardson number with model (3).

$$(P_\Delta)\quad \int_{-h}^{0} \frac{u_\Delta^{n+1}-u_\Delta^{n}}{\Delta t} w_\Delta + \int_{-h}^{0} f_1\left(R_\Delta^n\right)\partial_z u_\Delta^{n+1}\partial_z w_\Delta = L(w_\Delta),\quad \forall w_\Delta \in V_\Delta, \tag{18}$$

where:

$$L(w_\Delta) = \sigma_u\, w_\Delta(0) + \int_{-h}^{0} D_u\, w_\Delta. \tag{19}$$

On another hand, we also consider the implicit method:

Obtain $u_\Delta \in U_b + V_\Delta$ such that

$$(Q_\Delta)\quad \int_{-h}^{0} \frac{u_\Delta^{n+1}-u_\Delta^{n}}{\Delta t} w_\Delta + \int_{-h}^{0} f_1\left(R_\Delta^{n+1}\right)\partial_z u_\Delta^{n+1}\partial_z w_\Delta = L(w_\Delta),\quad \forall w_\Delta \in V_\Delta. \tag{20}$$

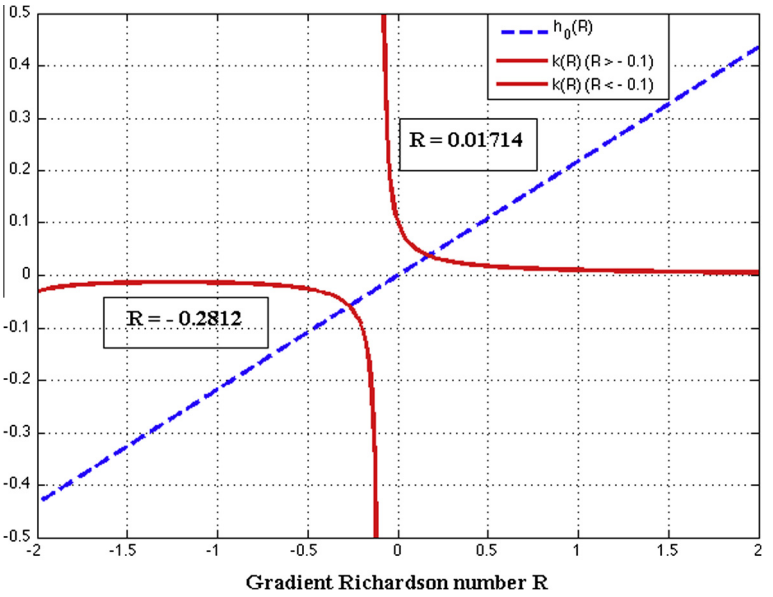

Fig. 3. Solution of the equation for equilibrium gradient Richardson number with model (4).

We consider similar discretizations for v and ρ. These discretizations were introduced in [5].

Both discretizations proposed, under certain hypotheses, are stable and verify a maximum principle. Denote by $\mathbf{U}_\Delta$ the continuous piecewise affine function from $[0,T]$ onto $[V_\Delta]^3$ whose value in t_n is $\mathbf{U}_\Delta^n = (u_\Delta^n, v_\Delta^n, \rho_\Delta^n)$, by $L^p(\mathbf{L}^q)$ the space $L^p((0,T);[L^q(I)]^3)$, and similarly the spaces $L^q(\mathbf{H}^k)$. We have the following:

Lemma 3.1. *Assume that the turbulent viscosities f_1, f_2 are uniformly bounded and positive. Then the discrete unsteady solution $\mathbf{U}_\Delta$ (in its semi-implicit and implicit version) satisfies:*

$$\|\mathbf{U}_\Delta\|_{L^\infty(\mathbf{L}^2)} + \|\mathbf{U}_\Delta\|_{L^2(\mathbf{H}^1)} + \|\partial_t \mathbf{U}_\Delta\|_{L^2(\mathbf{H}^{-1})} \leqslant C, \tag{21}$$

where C is a positive constant that only depends on the data (and not on Δz and Δt).

The proof of Lemma 3.1 is just the analogous of the one that can be found in [5] for the un-perturbed model. This result proves the stability of the discrete solutions in standard norms for parabolic problems.

Moreover, both discretizations (P_Δ) and (Q_Δ) verify a maximum principle, that we state without proof, as it is a standard result:

Lemma 3.2. *Assume $f_1 > 0$. If the data U_0, U_b and σ_u are positive, and D_u is positive or null, then u_Δ is positive in $[-h,0]\times[0,+\infty)$. If D_u is negative, then u_Δ is positive in a time interval $[0,T]$ such that $\|D_u\|_{L^\infty(I)} < \left(\min_{z\in\bar{I}} U_0(z)\right)/T$.*

Observe that if D_u is negative, it acts as an adverse pressure gradient. Then it will revert the direction of the velocity if it is applied for a long enough time. Similarly, it is possible to deduce this result for v_Δ.

The previous analysis presents some limitations. On one hand, the parabolic stability norms that appear in Lemma 3.1 are not strong enough to deduce the existence of solutions for the continuous problem (Cf. [7]). On another hand, the hypothesis that the turbulent viscosities are uniformly bounded is somewhat unrealistic, as in practice f_1 and f_2 are unbounded for $R < 0$. In the sequel, we shall develop a specific analysis for the actual turbulent viscosities corresponding to PP, Gent and Bennis et al. models, with much less restrictive conditions.

4. Analysis of discrete equilibria

In this section, we perform an analysis of the discrete equation and its relationship with the continuous one. We prove existence and uniqueness of discrete equilibrium, and its convergence to the continuous one as $\Delta z \to 0$. We also prove a result of practical interest: the continuous equilibria are asymptotically reached by the solutions of scheme (20) as $n \to +\infty$ and $\Delta z \to 0$. We assume the following:

Hypothesis 2. The turbulent viscosities $f_1, f_2 \in C^1([0,+\infty))$, and are uniformly bounded and positive for $R \geqslant 0$, that is:

$$\exists \quad 0 < \nu \leqslant M \quad \text{such that} \quad \nu \leqslant f_1(R), f_2(R) \leqslant M, \quad \forall R \geqslant 0.$$

The turbulent viscosities of the PP (3), Gent (4) and Bennis et al. (5) models satisfy Hyptohesis 2. Indeed, for PP and Bennis et al. models:

$$a_1 \leqslant f_1(R) \leqslant a_1 + b_1, \quad a_2 \leqslant f_2(R) \leqslant a_2 + a_1 + b_1, \quad \forall R \geqslant 0,$$

while for Gent model:

$$a_1 \leqslant f_1(R) \leqslant a_1 + b_1, \quad a_2 \leqslant f_2(R) \leqslant a_2 + b_1, \quad \forall R \geqslant 0.$$

4.1. Existence and uniqueness of discrete equilibria

We prove existence and uniqueness of discrete equilibrium solutions. The main problem that we face is that for zero gradient velocities, the gradient Richardson number is not defined. We prove that under Hypothesis 1, there exist an equilibrium with bounded (from above and from below) velocity gradient.

We reformulate the discrete steady problem as a system of algebraic equations for the unknowns:

$$\alpha_\Delta = \partial_z u_\Delta, \quad \beta_\Delta = \partial_z v_\Delta, \quad \theta_\Delta = \partial_z \rho_\Delta.$$

To do that, we define the piecewise constant finite element space:

$$G_\Delta = \left\{ \varphi_\Delta \in L^2(I) \text{ such that } \varphi_{\Delta|_{(z_{i-1}\, z_i)}} \text{ is constant, } i = 1, \ldots, N \right\}.$$

The equilibria of the discrete problem, if these exist, are solutions $(u^e_\Delta, v^e_\Delta, \rho^e_\Delta) \in (U_b, V_b, R_b) + [V_\Delta]^3$ of the non-linear system of equations:

$$\begin{cases} \int_{-h}^{0} f_1(R_\Delta)\, \partial_z u_\Delta \partial_z w_{1\Delta} = L_1(w_{1\Delta}), & \forall w_{1\Delta} \in V_\Delta, \\ \int_{-h}^{0} f_1(R_\Delta)\, \partial_z v_\Delta \partial_z w_{2\Delta} = L_2(w_{2\Delta}), & \forall w_{2\Delta} \in V_\Delta, \\ \int_{-h}^{0} f_2(R_\Delta)\, \partial_z \rho_\Delta \partial_z w_{3\Delta} = L_\rho(w_{3\Delta}), & \forall w_{3\Delta} \in V_\Delta, \end{cases} \tag{22}$$

where:

$$R_\Delta = -\frac{g}{\rho_r} \frac{\partial_z \rho_\Delta}{(\partial_z u_\Delta)^2 + (\partial_z v_\Delta)^2},$$

$$L_1(w_{1\Delta}) = \sigma_u\, w_{1\Delta}(0) + \int_{-h}^{0} D_u\, w_{1\Delta}, \quad L_2(w_{2\Delta}) = \sigma_v\, w_{2\Delta}(0) + \int_{-h}^{0} D_v\, w_{2\Delta},$$

$$L_\rho(w_{3\Delta}) = \sigma_\rho\, w_{3\Delta}(0) + \int_{-h}^{0} D_\rho\, w_{3\Delta}.$$

We prove that problem (22) is equivalent to:

$$(\alpha_\Delta, \beta_\Delta, \theta_\Delta) \in [G_\Delta]^3 \text{ such that } \begin{cases} \int_{-h}^{0} f_1(\widetilde{R}_\Delta)\, \alpha_\Delta \varphi_{1\Delta} = L_1(w(\varphi_{1\Delta})), & \forall \varphi_{1\Delta} \in G_\Delta, \\ \int_{-h}^{0} f_1(\widetilde{R}_\Delta)\, \beta_\Delta \varphi_{2\Delta} = L_2(w(\varphi_{2\Delta})), & \forall \varphi_{2\Delta} \in G_\Delta, \\ \int_{-h}^{0} f_2(\widetilde{R}_\Delta)\, \theta_\Delta \varphi_{3\Delta} = L_\rho(w(\varphi_{3\Delta})), & \forall \varphi_{3\Delta} \in G_\Delta, \end{cases} \tag{23}$$

where:

$$\widetilde{R}_\Delta = \widetilde{R}_\Delta(\alpha_\Delta, \beta_\Delta, \theta_\Delta) = -\frac{g}{\rho_r} \frac{\theta_\Delta}{(\alpha_\Delta)^2 + (\beta_\Delta)^2}, \quad (w(\varphi_\Delta))(z) = \int_{-h}^{z} \varphi_\Delta(s) ds \text{ (see Fig.4)}.$$

Lemma 4.1. *Problem (22) is equivalent to problem (23) in the sense that $(\alpha_\Delta, \beta_\Delta, \theta_\Delta)$ is a solution of (23) if and only if the triplet:*

$$u_\Delta(z) = U_b + \int_{-h}^{z} \alpha_\Delta(s) ds, \quad v_\Delta(z) = V_b + \int_{-h}^{z} \beta_\Delta(s) ds, \quad \rho_\Delta(z) = R_b + \int_{-h}^{z} \theta_\Delta(s) ds,$$

is a solution of (22).

Proof. On one hand, as $G_\Delta = \{\partial_z w_\Delta | w_\Delta \in V_\Delta\}$, if $(u_\Delta, v_\Delta, \rho_\Delta) \in (U_b, V_b, R_b) + [V_\Delta]^3$ is solution of problem (22), then $(\alpha_\Delta, \beta_\Delta, \theta_\Delta) \in [G_\Delta]^3$ is solution of problem (23). On another hand, if $(\alpha_\Delta, \beta_\Delta, \theta_\Delta) \in [G_\Delta]^3$ is solution of problem (23), as:

$$\begin{cases} \partial_z u_\Delta = \alpha_\Delta, & \partial_z v_\Delta = \beta_\Delta, & \partial_z \rho_\Delta = \theta_\Delta, \\ u_\Delta(-h) = U_b, & v_\Delta(-h) = V_b, & \rho_\Delta(-h) = R_b, \end{cases} \tag{24}$$

then $(u_\Delta, v_\Delta, \rho_\Delta) \in (U_b, V_b, R_b) + [V_\Delta]^3$ is solution of problem (22). □

To prove existence of discrete equilibria, we may refer to problem (23):

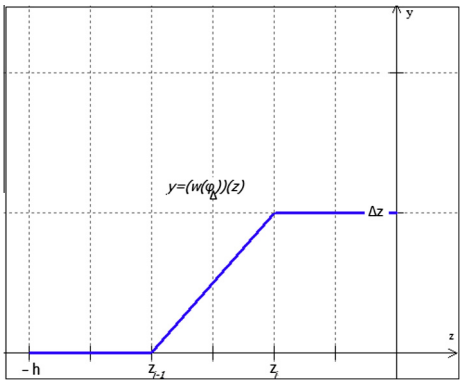

Fig. 4. Graphic of the function $y = (w(\varphi_\Delta))(z)$.

Theorem 4.1. *Under Hypotheses 1 and 2, problem (23) admits at least a solution that verifies:*

$$\alpha_\Delta > 0, \quad \beta_\Delta > 0, \quad \theta_\Delta < 0, \quad \text{and} \quad C_1 \leqslant |\alpha_\Delta|, |\beta_\Delta|, |\theta_\Delta| \leqslant C_2, \tag{25}$$

where:

$$C_1 = \frac{\lambda}{2M} \min\{Q_u, Q_v, |Q_\rho|\}, \quad C_2 = 3\,\frac{\lambda}{2\nu} \max\{Q_u, Q_v, |Q_\rho|\}. \tag{26}$$

Proof. We initially focus on the first component of the velocity. Let $\alpha_\Delta,\ \beta_\Delta,\ \theta_\Delta \in G_\Delta$. Assume that $\widetilde{R}_\Delta = \widetilde{R}_\Delta(\alpha_\Delta, \beta_\Delta, \theta_\Delta) > 0$. Consider the following linearization of the first equation of system (23):

$$\widehat{\alpha} \in G_\Delta \text{ such that } \int_{-h}^{0} f_1(\widetilde{R}_\Delta)\,\widehat{\alpha}_\Delta \varphi_{1\Delta} = L_1(w(\varphi_{1\Delta})), \quad \forall \varphi_{1\Delta} \in G_\Delta. \tag{27}$$

Problem (23) is exactly solved as follows:

Set $\widehat{\alpha}_\Delta = \sum_{i=1}^{N} \widehat{\alpha}_i \varphi_{1\Delta}$, where $\varphi_{1\Delta} = \mathbf{1}_{(z_{i-1}, z_i)} = \varphi_{1i} \in G_\Delta$, and $\mathbf{1}_{(z_{i-1}, z_i)}$ is the indicator function of the subinterval (z_{i-1}, z_i). Then, (27) becomes:

$$\widehat{\alpha}_i \int_{z_{i-1}}^{z_i} f_1(\widetilde{R}_\Delta) = L_1(w(\varphi_{1i})), \text{ for } i = 1, \ldots, N.$$

It implies that:

$$\widehat{\alpha}_i = \frac{L_1(w(\varphi_{1i}))}{\int_{z_{i-1}}^{z_i} f_1\left(\widetilde{R}_\Delta\right)}.$$

Observe that:

$$L_1(w(\varphi_{1i})) = \sigma_u\,(w(\varphi_{1i}))(0) + \int_{-h}^{0} D_u\, w(\varphi_{1i}),$$

$$(w(\varphi_{1i}))(z) = \int_{-h}^{z} \varphi_{1i}(s)ds = \begin{cases} 0, & \text{if } z < z_{i-1}; \\ z - z_{i-1}, & \text{if } z_{i-1} < z < z_i; \\ z_i - z_{i-1} = \Delta z, & \text{if } z > z_i. \end{cases}$$

Then, we obtain:

$$(w(\varphi_{1i}))(0) = \Delta z, \quad \int_{-h}^{0} D_u(z)\,(w(\varphi_{1i}))(z)dz = \int_{z_{i-1}}^{z_i} D_u(z)\,(z - z_{i-1})\,dz + \Delta z \int_{z_i}^{0} D_u(z)\,dz.$$

Moreover, we can write:

$$\int_{z_{i-1}}^{z_i} f_1(\widetilde{R}_\Delta) = \Delta z f_1(R_i), \text{ with } R_i = \widetilde{R}(\alpha_i, \beta_i, \theta_i).$$

Thus, we have:

$$\widehat{\alpha}_i = \frac{\sigma_u + \int_{z_{i-1}}^{z_i} D_u(z)\,(z - z_{i-1})/\Delta z\,dz + \int_{z_i}^{0} D_u(z)\,dz}{f_1(R_i)}. \tag{28}$$

As:

$$\left| \int_{z_{i-1}}^{z_i} D_u(z)\,(z - z_{i-1})/\Delta z\,dz + \int_{z_i}^{0} D_u(z)\,dz \right| \leqslant \|D_u\|_{L^1(I)},$$

using Hypothesis 1, we obtain:

$$\frac{\lambda}{2} Q_u \leqslant \sigma_u + \int_{z_{i-1}}^{z_i} D_u(z)\,(z - z_{i-1})/\Delta z\,dz + \int_{z_i}^{0} D_u(z)\,dz \leqslant 3\,\frac{\lambda}{2} Q_u.$$

Using Hypothesis 2, this implies that:

$$0 < \frac{\lambda}{2}\frac{Q_u}{M} \leqslant \widehat{\alpha}_\Delta \leqslant 3\,\frac{\lambda}{2}\frac{Q_u}{v}. \tag{29}$$

Similarly:

$$0 < \frac{\lambda}{2}\frac{Q_v}{M} \leqslant \widehat{\beta}_\Delta \leqslant 3\,\frac{\lambda}{2}\frac{Q_v}{v} \quad \text{and} \quad 3\,\frac{\lambda}{2}\frac{Q_\rho}{M} \leqslant \widehat{\theta}_\Delta \leqslant \frac{\lambda}{2}\frac{Q_\rho}{M} < 0. \tag{30}$$

Let us define the set:

$$K_\Delta(C_1, C_2) = \left\{ (w_{1\Delta}, w_{2\Delta}, w_{3\Delta}) \in [G_\Delta]^3 \text{ such that } C_1 \leqslant |w_{i\Delta}| \leqslant C_2,\ i = 1,2,3 \right\}, \tag{31}$$

where C_1 and C_2 are given by (26). The set $K_\Delta(C_1, C_2)$ is a non-empty convex compact subset of the finite-dimensional vector space $[G_\Delta]^3$. Let $\tau : K_\Delta(C_1, C_2) \to K_\Delta(C_1, C_2)$ be the map defined by:

$$\tau(\alpha_\Delta, \beta_\Delta, \theta_\Delta) = \left(\widehat{\alpha}_\Delta, \widehat{\beta}_\Delta, \widehat{\theta}_\Delta\right).$$

By (28), it is clear that τ is continuous. By applying Brouwer's fixed point theorem (Cf. [8]), it follows the existence of at least a solution of the discrete steady problem (23). □

We next step to the analysis of uniqueness of solution of problem (23). We state at first a technical result. We denote by $|\cdot|$ the Euclidean norm on $\mathbb{R}^m$.

Lemma 4.2. *Let the set:*

$$S = \left[\frac{\lambda}{2M} Q_u, \frac{3\lambda}{2v} Q_u\right] \times \left[\frac{\lambda}{2M} Q_v, \frac{3\lambda}{2v} Q_v\right] \times \left[\frac{3\lambda}{2v} Q_\rho, \frac{\lambda}{2M} Q_\rho\right]. \tag{32}$$

Then, for any $\mathcal{A}_1 = (\alpha_1, \beta_1, \theta_1),\ \mathcal{A}_2 = (\alpha_2, \beta_2, \theta_2) \in S$, *the following estimates hold:*

$$|f_1(R(\mathcal{A}_1)) - f_1(R(\mathcal{A}_2))| \leqslant K_1\,|\mathcal{A}_1 - \mathcal{A}_2|, \tag{33}$$

$$|f_2(R(\mathcal{A}_1)) - f_2(R(\mathcal{A}_2))| \leqslant K_2\,|\mathcal{A}_1 - \mathcal{A}_2|, \tag{34}$$

where:

$$R(\mathcal{A}_i) = -\frac{g}{\rho_r}\frac{\theta_i}{\alpha_i^2 + \beta_i^2}, \quad i = 1,2, \tag{35}$$

and:

$$K_1 = \frac{C}{(1+\overline{R})^3}\left(\frac{M^2}{\nu\lambda}\right)^2\left[\frac{(Q_u + Q_v)\overline{R} + 1}{Q_u^2 + Q_v^2}\right], \tag{36}$$

$$K_2 = \frac{C}{(1+\overline{R})^n}\left(\frac{M^2}{\nu\lambda}\right)^2\left[\frac{(Q_u + Q_v)\overline{R} + 1}{Q_u^2 + Q_v^2}\right], \tag{37}$$

with:

$$\overline{R} = \frac{|Q_\rho|}{Q_u^2 + Q_v^2}, \quad n = \begin{cases} 4 & \text{if} \quad f_1, f_2 \text{ are defined by (3), (4),} \\ 5 & \text{if} \quad f_1, f_2 \text{ are defined by (5),} \end{cases}$$

and C a numerical constant.

Proof. Observe that if $\mathcal{A} = (\alpha, \beta, \theta) \in S$, then the associated Richardson number $R = -\frac{g}{\rho_r}\frac{\theta}{\alpha^2+\beta^2}$ is positive. Then $f_1(R(\cdot))$ and $f_2(R(\cdot))$ are smooth functions on S. By the mean value theorem:

$$|f_1(R(\mathcal{A}_1)) - f_1(R(\mathcal{A}_2))| \leqslant ||f_1'||_{L^\infty(J)} |R(\mathcal{A}_1) - R(\mathcal{A}_2)| \leqslant ||f_1'||_{L^\infty(J)} |\nabla R(\mathcal{B})|\, |\mathcal{A}_1 - \mathcal{A}_2|, \tag{38}$$

for some $\mathcal{B}$ in the open segment of extremities $\mathcal{A}_1$ and $\mathcal{A}_2$, and J denoting the set:

$$J = \left[\frac{g}{\rho_r}\frac{2\nu}{3\lambda}\overline{R}, \frac{g}{\rho_r}\frac{2M}{\lambda}\overline{R}\right].$$

Assume for instance that f_1 and f_2 are given by (4). Then:

$$f_1'(R) = -20b_1(1+10R)^{-3}, \quad f_2'(R) = -30b_1(1+10R)^{-4};$$

$$\nabla R(\alpha,\beta,\theta) = \frac{g}{\rho_r}\left(2\alpha\theta(\alpha^2+\beta^2)^{-2},\ 2\beta\theta(\alpha^2+\beta^2)^{-2},\ -(\alpha^2+\beta^2)^{-1}\right).$$

By estimates (25) and (26), we deduce:

$$||f_1'||_{L^\infty(J)} \leqslant \frac{C_1}{(1+\overline{R})^3}, \quad ||f_2'||_{L^\infty(J)} \leqslant \frac{C_2}{(1+\overline{R})^4},$$

$$||\nabla R||_{L^\infty(S)} \leqslant C_3\left(\frac{M^2}{\nu\lambda}\right)^2\left[\frac{(Q_u+Q_\nu)\overline{R}+1}{Q_u^2+Q_\nu^2}\right],$$

where:

$$C_1 = 20\,b_1 \max\left\{\left(\frac{M}{\nu}\right)^2, \frac{9\lambda}{20}, \frac{M}{nu^2}\frac{\rho_r}{g}\right\}^3, \quad C_2 = 30\,b_1 \max\left\{\left(\frac{M}{\nu}\right)^2, \frac{9\lambda}{20}\frac{M}{nu^2}\frac{\rho_r}{g}\right\}^4, \quad C_3 = 72\,\frac{g}{\rho_r}.$$

Combining with (38), estimates (33) and (34) follow. When f_1 and f_2 are given by (3) and (5), estimates (33) and (34) follow in the same manner, as in these cases:

$$||f_1'||_{L^\infty(J)} \leqslant \frac{C_1}{(1+\overline{R})^3}, \quad ||f_2'||_{L^\infty(J)} \leqslant \frac{C_2}{(1+\overline{R})^n},$$

for some numerical constants $C_1, C_2 > 0$, and $n = 4, 5$ respectively for model (3), (5). These exponents are justified by the fact that we are interested in tropical seas, where usually $\overline{R} \sim 10^2$ (see Section 5.1), and so $R \in J \sim \left[\frac{2\cdot 10^{-5}\lambda}{3}, \frac{2\cdot 10^{-2}}{\lambda}\right]$, since $\frac{g}{\rho_r} \sim 10^{-2}$, and $\nu \sim 10^{-5}$, $M \sim 10^{-2}$ for model (3), (5). It implies that, at least for $\lambda \geqslant 10^{-1}$, $R \leqslant 0.2$, and from this follow the above exponents. □

We are now in a position to state our result of uniqueness of solution for problem (23).

Theorem 4.2. *Under Hypotheses 1 and 2, assume that the momentum fluxes Q_u, Q_ν remain bounded from above and from below. Then, for large enough negative surface heat fluxes Q_ρ, problem (23) admits a unique solution.*

Proof. Assume that α_Δ and α_Δ^1 are both solutions of the first equation of system (23). Let us set $\delta\alpha_\Delta = \alpha_\Delta - \alpha_\Delta^1$. As $\int_{-h}^0 f_1\left(\widetilde{R}_\Delta\right)\alpha_\Delta\varphi_{1\Delta} = \int_{-h}^0 f_1\left(\widetilde{R}_\Delta^1\right)\alpha_\Delta^1\varphi_{1\Delta}$, with obvious notation, we have:

$$\int_{-h}^0 f_1\left(\widetilde{R}_\Delta\right)\delta\alpha_\Delta\varphi_{1\Delta} = \int_{-h}^0\left[f_1\left(\widetilde{R}_\Delta^1\right) - f_1\left(\widetilde{R}_\Delta\right)\right]\alpha_\Delta^1\varphi_{1\Delta}, \quad \forall\varphi_{1\Delta} \in G_\Delta. \tag{39}$$

Using Lemma 4.2:

$$\int_{-h}^0 f_1\left(\widetilde{R}_\Delta\right)\delta\alpha_\Delta\varphi_{1\Delta} \leqslant K_1\int_{-h}^0 |\delta\mathcal{A}_\Delta|\,|\alpha_\Delta^1||\varphi_{1\Delta}|, \tag{40}$$

where $\delta\mathcal{A}_\Delta = (\alpha_\Delta^1 - \alpha_\Delta, \beta_\Delta^1 - \beta_\Delta, \theta_\Delta^1 - \theta_\Delta)$. Let $\varphi_{1\Delta} = \delta\alpha_\Delta$, so that, as $f_1 \geqslant a_1$, we obtain:

$$a_1\,||\delta\alpha_\Delta||_{L^2(I)} \leqslant K_1\,\|\delta\mathcal{A}_\Delta\|_{L^2(I)}\,||\alpha_\Delta^1||_{L^\infty(I)} \leqslant N_u\,\|\delta\mathcal{A}_\Delta\|_{L^2(I)}, \tag{41}$$

where $N_u = \frac{3\lambda}{2\nu}K_1Q_u$. Similarly:

$$a_1\,||\delta\beta_\Delta||_{L^2(I)} \leqslant N_\nu\,\|\delta\mathcal{A}_\Delta\|_{L^2(I)}, \tag{42}$$

where $N_\nu = \frac{3\lambda}{2\nu}K_1Q_\nu$, and:

$$a_2\,||\delta\theta_\Delta||_{L^2(I)} \leqslant N_\rho\,\|\delta\mathcal{A}_\Delta\|_{L^2(I)}, \tag{43}$$

where $N_\rho = \frac{3\lambda}{2\nu} K_2 |Q_\rho|$. Then, we can write:

$$\widehat{C}||\delta \mathcal{A}_\Delta||_{L^2(I)} \leqslant 0,$$

where:

$$\widehat{C} = \nu(1-N), \quad \nu = \min\{a_1, a_2\},$$

and:

$$N = \frac{C}{(1+\overline{R})^3}\left(\frac{M}{\nu}\right)^4 \left[\frac{(Q_u+Q_v)\overline{R}+1}{Q_u^2+Q_v^2}\right](Q_u+Q_v+|Q_\rho|), \tag{44}$$

for some numerical constant $C > 0$. Assuming $\sigma \leqslant Q_u, Q_v \leqslant \tau$ for some $0 < \sigma < \tau$, then the bound:

$$N \leqslant C\left(\frac{M}{\nu}\right)^4 \frac{1}{(1+\overline{R})^3}\left[3\overline{R} + \tau/\sigma^2 + 2\tau\overline{R}^2\right],$$

holds. Then, $N < 1$ if $|Q_\rho|$ is large enough, and consequently, the solution of the discrete problem (23) is unique. □

Remark 4.1. We have proved the uniqueness of solutions of the discrete model (23) for flows dominated by negative (warming) surface thermodynamic fluxes. This is coherent from a physical point of view, as the warming of the surface has a stabilizing effect on the mixing layer. The flow in the tropical seas fits into this case, as Q_ρ is typically negative. However, for all models, if we consider realistic values of the momentum and heat surface fluxes in tropical seas (see Section 5.1), the constant N defined by (44) is typically greater than one. Nevertheless, in a small neighbourhood of an equilibrium, the estimate for the constant N given by (44) can be directly replaced by an expression in terms of the equilibrium solution, and thus can be reduced enough, resulting to be effectively smaller than one for all models.

4.2. Convergence of discrete equilibrium to the continuous one

We next prove that the discrete equilibria converge to the continuous ones, for large enough negative surface heat fluxes. This analysis implies the existence of equilibria of problem (7,8) as weak solutions of the steady version of this problem, so as its stability with respect to numerical discretizations.

Theorem 4.3. *Assume that Hypotheses 1 and 2 hold, and that $D_u,\ D_v,\ D_\rho \in L^\infty(I)$. Assume also that the momentum fluxes $Q_u,\ Q_v$ remain bounded from above and from below. Then, for large enough negative surface heat fluxes Q_ρ, the sequence $\{(u_\Delta, v_\Delta, \rho_\Delta)\}_{\Delta z>0}$ is strongly convergent in $[H^1(I)]^3$ to a weak solution (u, v, ρ) of the steady version of problem (7,8).*

Proof. We prove that $\alpha_\Delta,\ \beta_\Delta,\ \theta_\Delta$ are BV (bounded variation) functions on $I = (-h, 0)$. Indeed, let us consider the total variation of α_Δ on I, that is defined as:

$$TV_{(I)}(\alpha_\Delta) = \sum_{i=1}^{N-1} |\alpha_{i+1} - \alpha_i|.$$

By identity (28) and Hypotheses 1 and 2, we have:

$$\begin{aligned}
|\alpha_{i+1} - \alpha_i| &= \left|\frac{\sigma_u + \frac{1}{\Delta z}\int_{-h}^0 D_u\, w_h(\varphi_{1,i+1})\,dz}{f_1(R_{i+1})} - \frac{\sigma_u + \frac{1}{\Delta z}\int_{-h}^0 D_u\, w_h(\varphi_{1,i})\,dz}{f_1(R_i)}\right| \\
&\leqslant |\sigma_u|\left|\frac{f_1(R_{i+1}) - f_1(R_i)}{f_1(R_{i+1})f_1(R_i)}\right| + \frac{1}{\Delta z}\left|\frac{\int_{-h}^0 D_u\left[w_h(\varphi_{1,i+1})f_1(R_i) - w_h(\varphi_{1,i})f_1(R_{i+1})\right]dz}{f_1(R_{i+1})f_1(R_i)}\right| \\
&\leqslant (2-\lambda)\frac{Q_u}{\nu^2}|f_1(R_{i+1}) - f_1(R_i)| + \frac{f_1(R_i)}{\Delta z\,\nu^2}\left|\int_{-h}^0 D_u\left[w_h(\varphi_{1,i+1}) - w_h(\varphi_{1,i})\right]dz\right| \\
&\quad + \frac{1}{\Delta z\,\nu^2}\left|\int_{-h}^0 D_u\, w_h(\varphi_{1,i})\,[f_1(R_i) - f_1(R_{i+1})]\,dz\right| \\
&\leqslant \frac{1}{\nu^2}\left[(2-\lambda)Q_u + \|D_u\|_{L^1(I)}\right]|f_1(R_{i+1}) - f_1(R_i)| + 2\,\frac{M}{\nu^2}\,\|D_u\|_{L^\infty(I)}\,\Delta z,
\end{aligned} \tag{45}$$

where the last inequality follows from $|w_h(\varphi_{1,i})| \leqslant \Delta z$ and from the estimate:

$$\begin{aligned}
&\left|\int_{-h}^0 D_u\left[w_h(\varphi_{1,i+1}) - w_h(\varphi_{1,i})\right]dz\right| \leqslant \left|\int_{z_i}^{z_{i+1}} D_u(z)\,(z - z_i)\,dz - \int_{z_{i-1}}^{z_i} D_u(z)\,(z - z_{i-1})\,dz\right| + \left|\int_{z_{i+1}}^0 D_u(z)\,\Delta z\,dz\right. \\
&\quad \left. - \int_{z_i}^0 D_u(z)\,\Delta z\,dz\right| \leqslant \|D_u\|_{L^\infty(I)}\Delta z^2 + \Delta z\int_{z_i}^{z_{i+1}} |D_u(z)|\,dz \leqslant 2\,\|D_u\|_{L^\infty(I)}\Delta z^2.
\end{aligned}$$

Recall that, by Theorem 4.1, for all $\Delta z > 0$ the triplet $(\alpha_\Delta, \beta_\Delta, \theta_\Delta)$ lies in the set S defined by (32). By Lemma 4.2:

$$|f_1(R_{i+1}) - f_1(R_i)| \leqslant K_1 \left[|\alpha_{i+1} - \alpha_i| + |\beta_{i+1} - \beta_i| + |\theta_{i+1} - \theta_i|\right],$$

where K_1 is given by (36). Combining this estimate with (45), we obtain:

$$|\alpha_{i+1} - \alpha_i| \leqslant L_1[|\alpha_{i+1} - \alpha_i| + |\beta_{i+1} - \beta_i| + |\theta_{i+1} - \theta_i|] + 2\,\frac{M}{\nu^2}\,\|D_u\|_{L^\infty(I)}\,\Delta z,$$

where $L_1 = \frac{C_1}{(1+\overline{R})^3}\left(\frac{M^2}{\nu^2\lambda}\right)^2\left[\frac{(Q_u+Q_v)\overline{R}+1}{Q_u^2+Q_v^2}\right]Q_u$. Similar estimates hold for $|\beta_{i+1} - \beta_i|$ and $|\theta_{i+1} - \theta_i|$, so we can write:

$$(1 - L_2)\sum_{i=1}^{N-1}(|\alpha_{i+1} - \alpha_i| + |\beta_{i+1} - \beta_i| + |\theta_{i+1} - \theta_i|) \leqslant L_3\sum_{i=1}^{N-1}\Delta z \leqslant L_3 h,$$

where:

$$L_2 = \frac{C_2}{(1+\overline{R})^3}\left(\frac{M^2}{\nu^2\lambda}\right)^2\left[\frac{(Q_u+Q_v)\overline{R}+1}{Q_u^2+Q_v^2}\right](Q_u + Q_v + |Q_\rho|),$$

for some numerical constant $C_2 > 0$, and:

$$L_3 = 2\,\frac{M}{\nu^2}\,(\|D_u\|_{L^\infty(I)} + \|D_v\|_{L^\infty(I)} + \|D_\rho\|_{L^\infty(I)}).$$

Arguing as in the proof of Theorem 4.2, the constant L_2 is smaller than one if Q_ρ is negative and large enough, then:

$$\sum_{i=1}^{N-1}(|\alpha_{i+1} - \alpha_i| + |\beta_{i+1} - \beta_i| + |\theta_{i+1} - \theta_i|) \leqslant \frac{L_3}{1 - L_2}h.$$

It implies that $\alpha_\Delta,\ \beta_\Delta,\ \theta_\Delta$ are uniformly bounded in $BV(I)$. As $BV(I)$ is compactly embedded in $L^1(I)$ (Cf. [9]), there exists a sub-sequence $\{(\alpha_{\Delta'}, \beta_{\Delta'}, \theta_{\Delta'})\}$ of $\{(\alpha_\Delta, \beta_\Delta, \theta_\Delta)\}$ strongly convergent in $[L^1(I)]^3$ to (α, β, θ). We deduce that there exists a sub-sequence of $\{(\alpha_{\Delta'}, \beta_{\Delta'}, \theta_{\Delta'})\}$, that we may denote in the same way, such that $(\alpha_{\Delta'}, \beta_{\Delta'}, \theta_{\Delta'}) \to (\alpha, \beta, \theta)$ a.e. in I. It follows that $f_1\left(\widetilde{R}_{\Delta'}\right) \to f_1(\widetilde{R})$ a.e. in I. At the same time, $\{f_1\left(\widetilde{R}_{\Delta'}\right)\}$ is bounded in $L^2(I)$, so that, up to a sub-sequence, $f_1\left(\widetilde{R}_{\Delta'}\right)$ weakly converges to a function g in $L^2(I)$. Let $\varphi \in L^2(I)$. For a positive constant C, we have:

$$|f_1\left(\widetilde{R}_{\Delta'}\right)||\varphi| \leqslant C|\varphi|, \quad f_1\left(\widetilde{R}_{\Delta'}\right)\varphi \to f_1(\widetilde{R})\varphi \text{ a.e. in } I.$$

By the dominated convergence theorem (Cf. [10]):

$$\int_{-h}^{0} f_1\left(\widetilde{R}_{\Delta'}\right)\varphi \to \int_{-h}^{0} f_1(\widetilde{R})\varphi.$$

As $f_1\left(\widetilde{R}_{\Delta'}\right) \to g$ in $L^2(I)$, we obtain:

$$\int_{-h}^{0}(f_1(\widetilde{R}) - g)\varphi = 0, \quad \forall\varphi \in L^2(I) \Rightarrow f_1(\widetilde{R}) = g.$$

So that, $f_1\left(\widetilde{R}_{\Delta'}\right) \to f_1(\widetilde{R})$ in $L^2(I)$. Moreover, for a positive constant C:

$$|f_1(\widetilde{R}_{\Delta'})|^2 \leqslant C, \quad |f_1(\widetilde{R}_{\Delta'})|^2 \to |f_1(\widetilde{R})|^2 \text{ a.e. in } I.$$

By the dominated convergence theorem:

$$||f_1\left(\widetilde{R}_{\Delta'}\right)||_{L^2(I)} \to ||f_1(\widetilde{R})||_{L^2(I)}.$$

It follows that $\left\{f_1\left(\widetilde{R}_{\Delta'}\right)\right\}$ strongly converges to $f_1(\widetilde{R})$ in $L^2(I)$. Let us consider $\varphi \in C^0(\bar{I})$. There exists a sequence $\{\varphi_{\Delta'}\}$ with $\varphi_{\Delta'} \in G_\Delta$ such that $\varphi_{\Delta'} \to \varphi$ in $L^\infty(I)$. Then:

$$f_1(\widetilde{R}_{\Delta'})\varphi_{\Delta'} \to f_1(\widetilde{R})\varphi \text{ in } L^2(I).$$

Finally, as $\alpha_{\Delta'} \to \alpha$ in $L^2(I)$, we can conclude:

$$\int_{-h}^{0} f_1\left(\widetilde{R}_{\Delta'}\right)\alpha_{\Delta'}\varphi_{\Delta'} \to \int_{-h}^{0} f_1(\widetilde{R})\alpha\varphi.$$

Then, $\{(u_{\Delta'}, v_{\Delta'}, \rho_{\Delta'})\}$ strongly converges in $[H^1(I)]^3$ to a weak solution (u, v, ρ) of the steady version of problem (1)–(6). Since we proved in Theorem 2.1 that (u, v, ρ) is unique, then the whole sequence $\{(u_\Delta, v_\Delta, \rho_\Delta)\}$ converges to it. □

Remark 4.2. It holds an analogous of Remark 4.1, i.e. the result of convergence holds for mixing layer flows dominated by negative (warming) surface thermodynamic fluxes.

4.3. Non-linear stability of discrete equilibria

We analyze in this section the asymptotic stability of the discrete equilibria. The objective is to prove that the continuous equilibria are well approximated by the solution of the evolutive discrete problems (18) and (20), which are computable in practice. We give a positive answer when the time iterates have bounded derivatives. Actually, we prove the asymptotic stability of the implicit discrete model (Q_Δ). We assume the following:

Hypothesis 3. The sequence $\{\partial_z \mathbf{U}_\Delta^n\}_{n\in\mathbb{N}}$ remains in the set S given by (32), for all $n \in \mathbb{N}$.

The proof of this hypothesis is actually in progress. Under this hypothesis, we prove the asymptotic stability of the implicit discrete model (Q_Δ). Let us denote by Π_Δ the standard nodal interpolate of continuous functions onto the space V_Δ.

Theorem 4.4. *Assume that Hypotheses 1–3 hold, and that* $D_u,\ D_v,\ D_\rho \in C^0(\bar{I})$. *Then, for large enough negative surface heat fluxes* Q_ρ, *and bounded (from above and from below) momentum fluxes* $Q_u,\ Q_v$, *the implicit discrete method* (Q_Δ) *is asymptotically stable, in the sense that:*

$$sup_{n\to+\infty}||\mathbf{U}_\Delta^n - \Pi_\Delta \mathbf{U}^e||_{L^2(I)} \leqslant C\Delta z, \tag{46}$$

where $\mathbf{U}_\Delta^n = (u_\Delta^n,\ v_\Delta^n,\ \theta_\Delta^n),\ \mathbf{U}^e = (u^e,\ v^e,\ \theta^e)$ *and* C *is a positive constant.*

Proof. Let us look for u_Δ^n as $u_\Delta^n = \Pi_\Delta u^e + \hat{u}_\Delta^n$, where $\hat{u}_\Delta^n$ is a perturbation. As $\Pi_\Delta u^e \in U_b + V_\Delta$, then $\hat{u}_\Delta^n \in V_\Delta$. If we set $\Pi_\Delta^* u^e = \Pi_\Delta u^e - u^e$, for all $w_\Delta \in V_\Delta$, we have that:

$$\int_{-h}^0 \frac{u_\Delta^{n+1} - u_\Delta^n}{\Delta t} w_\Delta + \int_{-h}^0 f_1\left(R_\Delta^{n+1}\right)\partial_z u_\Delta^{n+1}\partial_z w_\Delta = L(w_\Delta), \tag{47}$$

$$\int_{-h}^0 \frac{\Pi_\Delta u^e - \Pi_\Delta u^e}{\Delta t} w_\Delta + \int_{-h}^0 f_1(R^e)\partial_z \Pi_\Delta u^e \partial_z w_\Delta = L(w_\Delta) + \int_{-h}^0 f_1(R^e)\partial_z \Pi_\Delta^* u^e \partial_z w_\Delta. \tag{48}$$

We take the difference between (47) and (48), and we add and subtract the quantity:

$$\int_{-h}^0 f_1\left(R_\Delta^{n+1}\right)\partial_z \Pi_\Delta u^e \partial_z w_\Delta.$$

We obtain:

$$\int_{-h}^0 (\hat{u}_\Delta^{n+1} - \hat{u}_\Delta^n) w_\Delta + \Delta t \int_{-h}^0 f_1\left(R_\Delta^{n+1}\right)\partial_z \hat{u}_\Delta^{n+1}\partial_z w_\Delta = \Delta t \int_{-h}^0 \left[f_1(R^e) - f_1\left(R_\Delta^{n+1}\right)\right]\partial_z \Pi_\Delta u^e \partial_z w_\Delta - \Delta t \int_{-h}^0 f_1(R^e)\partial_z \Pi_\Delta^* u^e \partial_z w_\Delta. \tag{49}$$

Let us take $w_\Delta = \hat{u}_\Delta^{n+1}$. Using the identity $(a-b)a = \frac{1}{2}|a|^2 - \frac{1}{2}|b|^2 + \frac{1}{2}|a-b|^2$, we deduce:

$$||\hat{u}_\Delta^{n+1}||_{L^2(I)}^2 + ||\hat{u}_\Delta^{n+1} - \hat{u}_\Delta^n||_{L^2(I)}^2 + 2\nu\Delta t||\partial_z \hat{u}_\Delta^{n+1}||_{L^2(I)}^2 \leqslant ||\hat{u}_\Delta^n||_{L^2(I)}^2 + 2\Delta t \int_{-h}^0 \left[f_1(R^e) - f_1\left(R_\Delta^{n+1}\right)\right]\partial_z \Pi_\Delta u^e \partial_z \hat{u}_\Delta^{n+1}$$
$$- 2\Delta t \int_{-h}^0 f_1(R^e)\partial_z \Pi_\Delta^* u^e \partial_z \hat{u}_\Delta^{n+1},$$

where we have used $f_1\left(R_\Delta^{n+1}\right) \geqslant \nu > 0$ from Hypotheses 2 and 3. By Lemma 4.2, we have:

$$\int_{-h}^0 \left[f_1(R^e) - f_1\left(R_\Delta^{n+1}\right)\right]\partial_z \Pi_\Delta u^e \partial_z \hat{u}_\Delta^{n+1} \leqslant K_1 \left|\left|\partial_z\left(\mathbf{U}^e - \mathbf{U}_\Delta^{n+1}\right)\right|\right|_{L^2(I)} ||\partial_z \Pi_\Delta u^e||_{L^\infty(I)} ||\partial_z \hat{u}_\Delta^{n+1}||_{L^2(I)},$$

where K_1 is defined by (36). From (14) and Hypothesis 1, it follows:

$$||\partial_z \Pi_\Delta u^e||_{L^\infty(I)} \leqslant ||\partial_z u^e||_{L^\infty(I)} \leqslant 2\frac{Q_u}{\nu},$$

so that:

$$\int_{-h}^0 \left[f_1(R^e) - f_1\left(R_\Delta^{n+1}\right)\right]\partial_z \Pi_\Delta u^e \partial_z \hat{u}_\Delta^{n+1} \leqslant L_u ||\partial_z\left(\mathbf{U}^e - \mathbf{U}_\Delta^{n+1}\right)||_{L^2(I)} ||\partial_z \hat{u}_\Delta^{n+1}||_{L^2(I)}$$
$$\leqslant L_u \left(||\partial_z \Pi_\Delta^* \mathbf{U}^e||_{L^2(I)} + ||\partial_z \hat{\mathbf{U}}_\Delta^{n+1}||_{L^2(I)}\right) ||\partial_z \hat{u}_\Delta^{n+1}||_{L^2(I)},$$

where we denote $L_u = 2K_1 \frac{Q_u}{\nu}$. Then:

$$||\hat{u}_\Delta^{n+1}||^2_{L^2(I)} + 2\nu\Delta t||\partial_z\hat{u}_\Delta^{n+1}||^2_{L^2(I)} \leqslant ||\hat{u}_\Delta^{n}||^2_{L^2(I)} + 2\Delta t L_u||\partial_z\hat{\mathbf{U}}_\Delta^{n+1}||_{L^2(I)}||\partial_z\hat{u}_\Delta^{n+1}||_{L^2(I)} + 2\Delta t\,(L_u||\partial_z\Pi_\Delta^*\mathbf{U}^e||_{L^2(I)} + M||\partial_z\Pi_\Delta^* u^e||_{L^2(I)})||\partial_z\hat{u}_\Delta^{n+1}||_{L^2(I)},$$

as $f_1(R^e) \leqslant M$ from Hypothesis 2. Similar estimates apply to the perturbations:

$$\hat{v}_\Delta^{n+1} = v_\Delta^n - \Pi_\Delta v^e, \quad \hat{\theta}_\Delta^{n+1} = \theta_\Delta^n - \Pi_\Delta\theta^e.$$

Summing these up, we deduce:

$$||\hat{\mathbf{U}}_\Delta^{n+1}||^2_{L^2(I)} + 2\nu\Delta t||\partial_z\hat{\mathbf{U}}_\Delta^{n+1}||^2_{L^2(I)} \leqslant ||\hat{\mathbf{U}}_\Delta^{n}||^2_{L^2(I)} + 2\Delta t L||\partial_z\hat{\mathbf{U}}_\Delta^{n+1}||^2_{L^2(I)} + 2\Delta t\,(L+M)||\partial_z\Pi_\Delta^*\mathbf{U}^e||_{L^2(I)}||\partial_z\hat{\mathbf{U}}_\Delta^{n+1}||_{L^2(I)},$$

where:

$$L = 2K_1\frac{Q_u+Q_v}{\nu} + 2K_2\frac{|Q_\rho|}{\nu} \leqslant \frac{C}{\nu(1+\overline{R})^3}\left(\frac{M^2}{\nu^2\lambda}\right)^2\left[\frac{(Q_u+Q_v)\overline{R}+1}{Q_u^2+Q_v^2}\right](Q_u+Q_v+|Q_\rho|),$$

and K_2 is defined by (37). Thus, for large enough $|Q_\rho|$, and bounded (from above and from below) $Q_u,\ Q_v$, we have $L < \nu$. Then, denoting $\widehat{\nu} = \nu - L$, we obtain:

$$||\hat{\mathbf{U}}_\Delta^{n+1}||^2_{L^2(I)} + 2\,\widehat{\nu}\,\Delta t||\partial_z\hat{\mathbf{U}}_\Delta^{n+1}||^2_{L^2(I)} \leqslant ||\hat{\mathbf{U}}_\Delta^{n}||^2_{L^2(I)} + 2\Delta t\,(L+M)||\partial_z\Pi_\Delta^*\mathbf{U}^e||_{L^2(I)}||\partial_z\hat{\mathbf{U}}_\Delta^{n+1}||_{L^2(I)}.$$

Using Young's inequality:

$$||\hat{\mathbf{U}}_\Delta^{n+1}||^2_{L^2(I)} + \widehat{\nu}\,\Delta t||\partial_z\hat{\mathbf{U}}_\Delta^{n+1}||^2_{L^2(I)} \leqslant ||\hat{\mathbf{U}}_\Delta^{n}||^2_{L^2(I)} + \Delta t\,\frac{(L+M)^2}{\widehat{\nu}}||\partial_z\Pi_\Delta^*\mathbf{U}^e||^2_{L^2(I)} \leqslant ||\hat{\mathbf{U}}_\Delta^{n}||^2_{L^2(I)} + C_1(\Delta z)^2\Delta t, \tag{50}$$

for some constant $C_1 > 0$, where the last inequality follows from the finite element interpolation error estimate:

$$||\partial_z\Pi_\Delta^*\mathbf{U}^e||_{L^2(I)} \leqslant C_2\Delta z||\partial_{zz}\mathbf{U}^e||_{L^2(I)},$$

for some numerical constant C_2. Here, we use the fact that $\mathbf{U}^e \in [C^2(\bar{I})]^3$ from (11), as $D_u,\ D_v,\ D_\rho \in C^0(\bar{I})$. Using Poincaré inequality $||\hat{\mathbf{U}}_\Delta^n||^2_{L^2(I)} \leqslant C_3||\partial_z\hat{\mathbf{U}}_\Delta^n||^2_{L^2(I)}$ for some constant $C_3 > 0$, we deduce from (50):

$$(1 + C_3\,\widehat{\nu}\Delta t)\sigma_{n+1} \leqslant \sigma_n + C_1(\Delta z)^2\Delta t.$$

where we denote $\sigma_n = ||\hat{\mathbf{U}}_\Delta^n||^2_{L^2(I)}$. Let $K = \frac{1}{(1+C_3\,\widehat{\nu}\Delta t)}$, so we can write:

$$\sigma_{n+1} \leqslant K\sigma_n + KC_1(\Delta z)^2\Delta t = (1 - C_4\Delta t)\sigma_n + (1 - C_4\Delta t)\,C_1(\Delta z)^2\Delta t, \tag{51}$$

where we denote $C_4 = C_3 K\,\widehat{\nu}$. Then:

$$\sigma_{n+1} \leqslant (1 - C_4\Delta t)^{n+1}\sigma_0 + (C_1/C_4)(\Delta z)^2, \tag{52}$$

and we conclude (46). □

We finally may state:

Corollary 4.1. *Under the hypotheses of Theorem 4.4, the sequence* $\{\mathbf{U}_\Delta^n\}_{n\in\mathbb{N}}$ *asymptotically converges to the continuous equilibrium* $\mathbf{U}^e$ *in* $[L^2(I)]^3$ *as* $(n, \Delta z) \to (+\infty, 0)$.

4.4. Numerical tests

We have performed some numerical tests to analyze the stability of the continuous equilibria (11), so as the convergence of the discrete steady states computed with model 18,19 to the continuous ones.

We initialize the code with the initial conditions shown in Fig. 5. These conditions correspond to data taken from the Tropical Atmosphere Ocean (TAO) array (Cf. [11]). We impose the boundary conditions $u_a = 11.7\ \mathrm{m}\cdot\mathrm{s}^{-1}$ (eastward wind), $v_a = 0.4\ \mathrm{m}\cdot\mathrm{s}^{-1}$ (northward wind) and $Q_\rho = -10^{-6}\ \mathrm{kg}\cdot\mathrm{m}^{-2}\cdot\mathrm{s}^{-1}$ (heat flux), typical values in tropical seas (Cf. [12,13]). In practice, the unsteady solutions corresponding to time $T = 10,000$ hours (about 14 months) change very little as time increases, so we consider them as steady solutions.

We present the results corresponding to model (5), by setting $\Delta z = 1$ m, $\Delta t = 1$ hour $= 3\,600$ s. Smaller values of Δz and Δt provide quite similar results. We consider the case $D_u = D_v = D =$ *constant*, with the following values: $D = 10^{-6}\ \mathrm{m}\cdot\mathrm{s}^{-2}$, $D = 0\ \mathrm{m}\cdot\mathrm{s}^{-2}$. The results are presented in Figs. 6 and 7.

On Fig. 6, we can observe in both cases a monotonic numerical convergence to the steady state, by computing the residual values as:

$$r^n = \left[\sum_{i=0}^{N}(|u_{z_i}^{n+1} - u_{z_i}^n|^2 + |v_{z_i}^{n+1} - v_{z_i}^n|^2 + |\rho_{z_i}^{n+1} - \rho_{z_i}^n|^2)\right]^{1/2}.$$

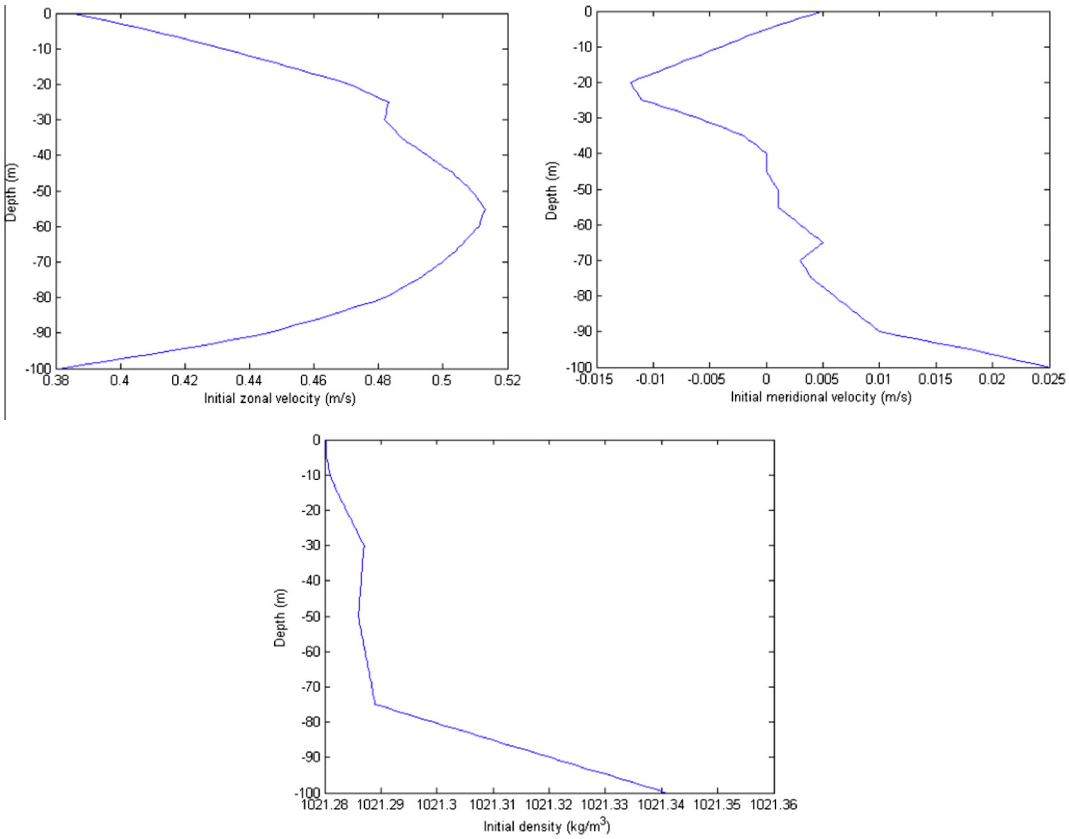

Fig. 5. Initial zonal velocity (top left), meridional velocity (top right) and density (bottom).

Really, already after $T = 1\,500$ hours (about 2 months), we reach a stable equilibrium, for which $r^n < 10^{-6}$. Collecting data at time $T = 10,000$ hours implies to consider a subsequent relaxation time, until to obtain $r^n \sim 10^{-12}$. On Fig. 7, at first we observe that the theoretical and the numerical solutions are very close. Also, for $D = 0\ \mathrm{m}\cdot\mathrm{s}^{-2}$ we effectively obtain linear profiles for both equilibrium velocity and density, as in Bennis et al. [5]. For $D = 10^{-6}\ \mathrm{m}\cdot\mathrm{s}^{-2}$ the density does not practically change its linear profile, while the zonal and the meridional velocities are largely changed.

We also test the convergence order of the iterates of the numerical scheme to the continuous equilibria, as stated in Corollary 4.1. Note that this result is based upon the hypothesis that the time iterates lie in a small enough neighbourhood of the equilibrium. Our results are presented in Table 1, where we confirm the thesis of Corollary 4.1: The time iterates of the numerical scheme approximate, for large enough time, the continuous equilibria, with order 1, in the sense that $||\mathbf{U}^n_\Delta - \mathbf{U}^e||_{L^2(I)} \simeq C\,\Delta z$ for large enough n. Actually, the convergence order deteriorates as Δz decreases, due to the error term coming from the time discretization in estimate (52).

5. Stability with respect to 2D perturbations

We perform in this section a numerical investigation of the finite-time stability of the algebraic mixing-layer models (3)–(5) with respect to 2D perturbations. Our procedure is to solve a 2D model of oceanic flow whose data are 1D plus a small 2D perturbation. In practice, 1D models are coupled to 3D models for the inner oceanic flows, so the 1D model may be affected by multi-dimensional perturbations. We test here whether replacing a multidimensional modeling of the mixing layer by a 1D mixing-layer model provides accurate results. We observe that the finite-time solutions provided by the 2D model loose memory of the 2D perturbation, and are close to the solutions provided by the 1D mixing-layer model. We consider characteristic times associated to the formation of mixing-layer profiles (almost constant density from the surface down to a depth where a sharp gradient appears), typically of the order of two days.

As 2D model of oceanic flow, we use the Primitive Equations. These govern oceanic flows at large scales in space and time, and are often used as a physical–mathematical basic model to analyze global climate changes and oceanic biosystems, usually in combination with turbulence models (Cf. [14]). In their reduced formulation, they form a set of PDEs for horizontal velocity, surface pressure and density, arising from the Boussinesq Equations together with the hydrostatic approximation.

Let us consider the 1D domain:

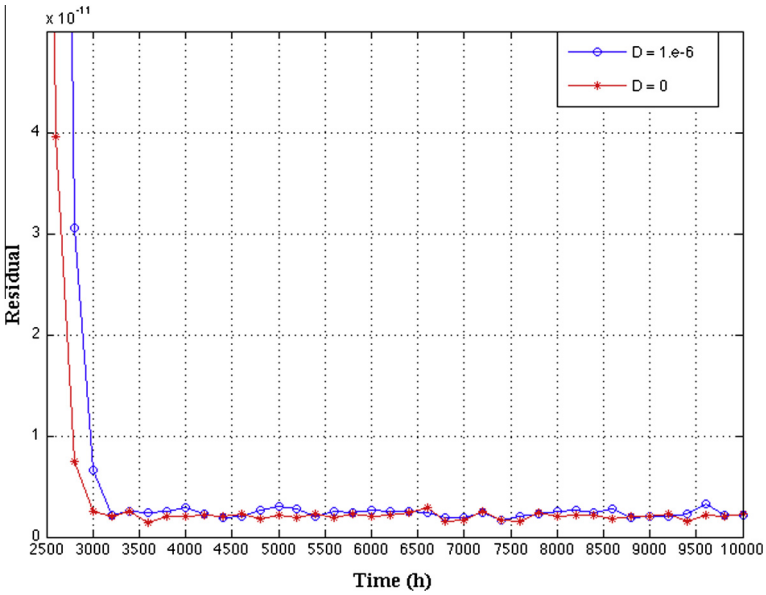

Fig. 6. Temporal evolution of residual values.

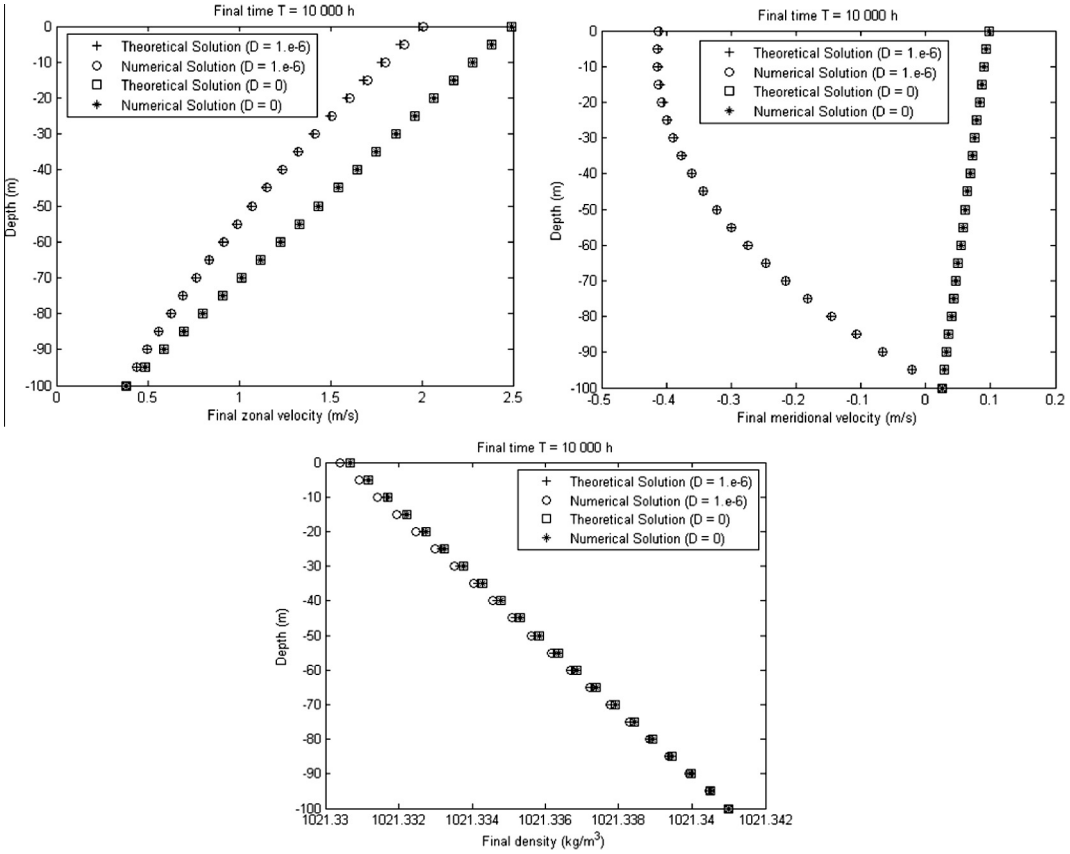

Fig. 7. Comparison of numerical solutions computed at $T = 10,000$ hours (about 14 months) and theoretical equilibria.

Table 1
Estimated error and convergence order.

Δz (m)	Final time $T = 10,000$ h, $D = 10^{-6}$ m · s^{-2}	
	$\|\|\mathbf{U}^n_\Delta - \mathbf{U}^e\|\|_{L^2(I)}$	Convergence order
8	0.7895	–
4	0.3893	1.02
2	0.2048	0.93
1	0.1149	0.83
0.5	0.0733	0.65

$$\omega = (0, L),\ L > 0,$$

that shall represent the rigid-surface domain of the flow. We define the 2D flow domain as:

$$\Omega = \{(x,z) \in \mathbb{R}^2 \text{ such that } x \in \omega,\ -h < z < 0\}.$$

We assume that the flow is homogeneous in the y direction and turbulent, and we represent by:

$$\mathbf{U} = (u(x,z;t), w(x,z;t)), \quad \rho = \rho(x,z;t), \quad p = p(x,z;t),$$

the mean velocity, density and pressure of the fluid, arising from a statistical Reynolds averaging of the 2D Boussinesq Equations. The averaged form of the Primitive Equations is:

$$\begin{cases} \nabla \cdot \mathbf{U} = 0, \\ \partial_t u + (\mathbf{U} \cdot \nabla) u - a_1 \Delta u + \partial_x p = -\nabla \cdot \langle \mathbf{U}' u' \rangle, \\ \partial_z p = -\frac{\rho}{\rho_r} g, \\ \partial_t \rho + (\mathbf{U} \cdot \nabla)\rho - a_2 \Delta \rho = -\nabla \cdot \langle \mathbf{U}' \rho' \rangle. \end{cases} \tag{53}$$

As we are considering tropical seas, we neglect the Coriolis force. Also, the anisotropy of the domain ($L \gg h$) permits to apply the hydrostatic approximation:

$$\partial_z p = -\frac{\rho}{\rho_r} g.$$

In system (53), U', u', and ρ' are respectively the fluctuations of the total velocity, the horizontal velocity and the density of the fluid, and a_1, a_2 are the laminar viscosity and diffusion. To solve the closure problem for model (53), we use the concept of eddy viscosity and diffusion. So, we set:

$$-\langle \mathbf{U}' u' \rangle = (\nu_h^t \partial_x u,\ \nu_v^t \partial_z u), \quad -\langle \mathbf{U}' \rho' \rangle = (k_h^t \partial_x \rho,\ k_v^t \partial_z \rho),$$

where ν_h^t and ν_v^t are the horizontal and vertical eddy viscosity coefficients, while k_h^t and k_v^t are the horizontal and vertical eddy diffusivity coefficients. We apply a Smagorinsky turbulence model for the horizontal eddy viscosity and diffusivity coefficients ν_h^t and k_h^t. The Smagorinsky turbulence model is a LES (Large Eddy Simulation) model based upon the eddy viscosity and mixing length concepts, intrinsically linked to a discretization grid (Cf. [15]). We consider:

$$\nu_h^t = (C_s \Delta x)^2 |\partial_x u|, \quad k_h^t = \frac{a_2}{a_1} \nu_h^t,$$

where C_s is the Smagorinsky constant, estimated from experimental measurements (Cf. [16]), and Δx is the horizontal turbulent mixing length, identified with the horizontal diameter of the elements of the grid considered on the computational domain Ω. As for the vertical eddy viscosity and diffusivity coefficients ν_v^t and k_v^t, we use the previous gradient Richardson number-based model (5). So, we consider:

$$\nu_v^t = \frac{b_1}{(1+5R)^2}, \quad k_v^t = \frac{a_1}{(1+5R)^2} + \frac{\nu_v^t}{(1+5R)^2},$$

where the gradient Richardson number R is now defined as:

$$R = -\frac{g}{\rho_r} \frac{\partial_z \rho}{(\partial_z u)^2}.$$

Let us decompose the boundary of Ω into four pieces, $\partial\Omega = \Gamma_b \cup \Gamma_s \cup \Gamma_{\ell 1} \cup \Gamma_{\ell 2}$, where Γ_b is the domain bottom, Γ_s is the Ocean surface, and $\Gamma_{\ell 1}$, $\Gamma_{\ell 2}$ are the vertical sidewalls. The hydrostatic and the rigid-lid assumptions allow to integrate the hydrostatic equation from an arbitrary depth z up to the rigid-surface $z = 0$:

$$\int_z^0 \partial_s p(x,s;t) ds = -\frac{g}{\rho_r} \int_z^0 \rho(x,s;t) ds \Rightarrow p(x,z;t) = p_s(x;t) + \frac{g}{\rho_r} \int_z^0 \rho(x,s;t) ds,$$

with p_s denoting the surface pressure. It follows that the horizontal gradient of the pressure is rewritten in terms of the horizontal gradient of the surface pressure, plus a baroclinic contribution:

$$\partial_x p(x,z;t) = \partial_x p_s(x;t) + \frac{g}{\rho_r}\partial_x \int_z^0 \rho(x,s;t)ds.$$

We consider the following initial-boundary value problem for the Primitive Equations:

$$\begin{cases} (a)\,\partial_t u + (\mathbf{U}\cdot\nabla)u - \partial_x(\nu_h\partial_x u) - \partial_z(\nu_v\partial_z u) + \partial_x p_s + (g/\rho_r)\partial_x\int_z^0 \rho(x,s;t)ds = 0 & \text{in } \Omega\times]0,T[,\\ (b)\,\partial_t\rho + (\mathbf{U}\cdot\nabla)\rho - \partial_x(k_h\partial_x\rho) - \partial_z(k_v\partial_z\rho) = 0 & \text{in } \Omega\times]0,T[,\\ (c)\,\partial_z w = -\partial_x u & \text{in } \Omega\times]0,T[,\\ (d)\,u_{|\Gamma_b} = u_b,\ \rho_{|\Gamma_b} = \rho_b & \text{in } [0,T],\\ (e)\,w_{|\Gamma_b} = w_{|\Gamma_s} = 0 & \text{in } [0,T],\\ (f)\,u_{|\Gamma_{\ell 1}} = u_{|\Gamma_{\ell 2}},\ \rho_{|\Gamma_{\ell 1}} = \rho_{|\Gamma_{\ell 2}} & \text{in } [0,T],\\ (g)\,\nu_v\partial_z u_{|\Gamma_s} = Q_u,\ k_v\partial_z\rho_{|\Gamma_s} = Q_\rho & \text{in } [0,T],\\ (h)\,u(0) = u_0,\ \rho(0) = \rho_0,\ w(0) = 0 & \text{in } \Omega, \end{cases} \tag{54}$$

where $\nu_h = a_1 + \nu_h^t,\ \nu_v = a_1 + \nu_v^t$ respectively are the total horizontal and vertical viscosity, and $k_h = a_2 + k_h^t,\ k_v = a_2 + k_v^t$ respectively are the total horizontal and vertical diffusion.

The boundary condition (54)-(*e*) includes the rigid-lid assumption: $w = 0$ at the surface $z = 0$. This model does not include a free-surface. The boundary condition (54)-(f) represents periodic boundary conditions that we impose on the sidewalls $\Gamma_{\ell 1},\ \Gamma_{\ell 2}$. These boundary conditions are physically reasonable. The remaining boundary conditions are those of the 1D model (1)–(6).

Remark 5.1. If the initial conditions are 1D (do not depend on x), the solutions of the mixing-layer models are solutions of the Primitive Equations with a zero pressure gradient.

We have discretized model (54) with a Galerkin FEM (finite element method) in the spatial variables, and a semi-implicit Euler scheme for the temporal variable. We have used $(P2 - P1)$ discretization for velocity–pressure. This ensures the stability of the discretization of the pressure (Cf. [17]). We also have used a $P1$ discretization for the density.

5.1. Numerical tests

We have solved the Primitive Equations (54) on the rectangular computational domain Ω, with a length $L = 3000$ m, and a thickness $h = 100$ m. We have set periodic 2D perturbations of the 1D initial conditions, of the form:

$$u(0) = u_0(z) + \lambda\sigma(x), \quad \rho(0) = \rho_0(z) + \lambda\sigma(x) \text{ in } \Omega, \tag{55}$$

by choosing a small λ. It permits to set genuine 2D initial conditions for the current problem (54). The initial 1D zonal velocity u_0 and density ρ_0 profiles are typical of tropical seas, and are taken from the Tropical Atmosphere Ocean (TAO) array (Cf. [11,12]).

We have performed two tests, respectively corresponding to physically unstable and physically stable initial conditions (inverse and favorable density gradients). We have constructed on Ω a uniform regular mesh, with horizontal and vertical

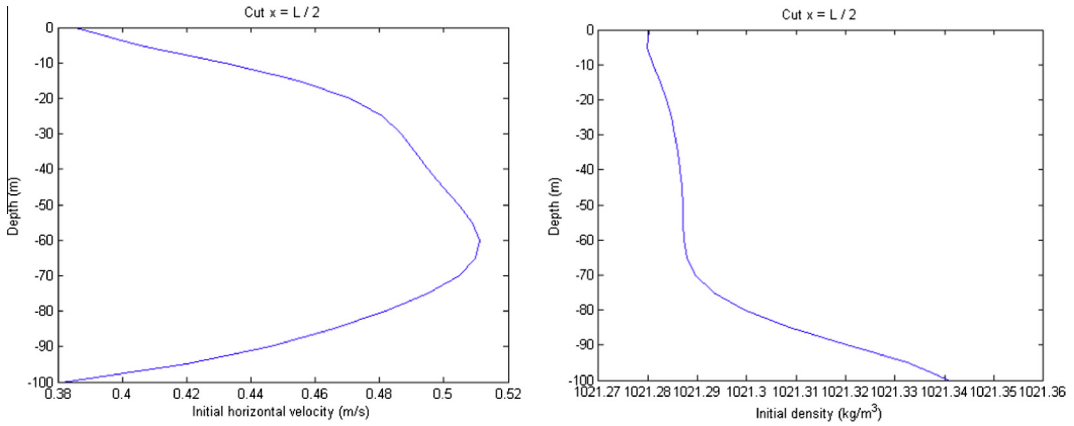

Fig. 8. Test 1: Initial horizontal velocity and density profiles (from left to right) at $x = L/2$.

grid sizes $\Delta x = 15$ m, $\Delta z = 1$ m. We have used the application FreeFem++ to implement the practical solution of the problem (Cf. [18]).

5.2. Test 1

The first test corresponds to an instability zone below the Ocean surface, where $\partial_z \rho > 0$ (see Fig. 8, where we show the initial horizontal velocity and density profiles for $x = L/2$).

As for the boundary conditions, we impose a heat flux $Q_\rho = -10^{-6}$ kg $\cdot$ m$^{-2}\cdot$ s^{-1}, and a zonal wind-stress $V_x \simeq 10^{-1}$ m$^{-2}\cdot$ s^{-2}, that are typical values for the Equatorial Pacific region, called West-Pacific Warm Pool (Cf. [4]). We integrate the 2D model for a final time $T = 48$ hours, with $\Delta t = 60$ s. In order to perform a comparison with the results of the 1D model, we compute it with the same data, by neglecting the meridional velocity, which is usually smaller than the zonal one.

Fig. 9 shows a comparison between the final horizontal velocity (on the left) and the final density (on the right) computed by the 2D model at $x = L/2$, and the 1D model 18,19 with $D_u = D = 10^{-7}$ m $\cdot$ s^{-2}, and $D_u = D = 0$ m $\cdot$ s^{-2}. The order of magnitude for D is found by observing that it plays the role of a horizontal pressure gradient, that may compensate for a loss of incompressibility in the initial conditions. Indeed, it is computed by the well-known *Bernoulli's law* applied to the initial velocity field along flow lines:

$$\frac{1}{2}|\mathbf{U}(0)|^2 + p = C,$$

where C is a constant, and then:

$$|D| = |\partial_x p| = |u(0)\partial_x u(0)|.$$

We consider the standard definition of mixed layer (Cf. [19]), that states that the base of the mixed layer is the depth at which the density changes by 0.01 kg $\cdot$ m^{-3}. From the final density profile we observe the formation of a mixed layer (almost constant density) of about 70 m depth, by using either the 2D model or the 1D model with a zero and non-zero pressure gradient D. A pycnocline (high gradient of density) is formed immediately below. This is a characteristic density profile for a well-mixed layer.

The final fluid velocity and density obtained with the 2D model are horizontally homogeneous, even starting from 2D initial conditions. Moreover, the vertical component of the velocity is almost zero. The final surface pressure, shown in Fig. 10, assumes its values in the range $[-2\cdot 10^{-7}, 2\cdot 10^{-7}]$.

The results of Fig. 9 stress that if we take into account a non-zero horizontal pressure gradient D in the 1D model, we barely improve the accuracy in the mixing-layer profiles, with respect to the mixing-layer profiles obtained with the 2D model. This not only shows the stability of the 1D model with respect to 2D perturbation, but also its accuracy to compute the mixing layer.

5.3. Test 2

The second test corresponds to a stable initial density profile (see Fig. 11).

As for the boundary conditions, we impose a heat flux $Q_\rho = -10^{-6}$ kg $\cdot$ m$^{-2}\cdot$ s^{-1}, and a zonal wind-stress $V_x \simeq 10^{-1}$ m$^{-2}\cdot$ s^{-2}. We integrate the 2D model for a final time $T = 24$ hours, with $\Delta t = 60$ s. In order to perform a comparison with the results of the 1D model, we compute it with the same data.

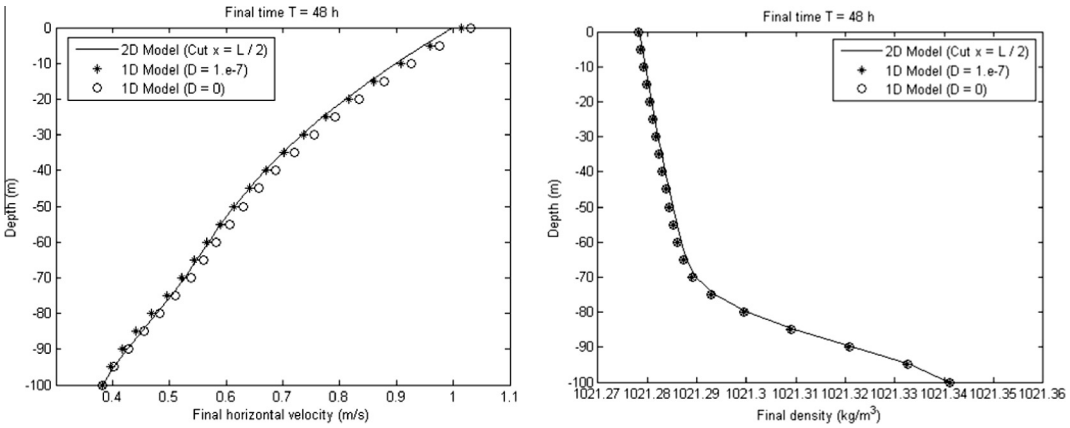

Fig. 9. Test 1: Comparison between 2D and 1D final horizontal velocity (left) and density (right).

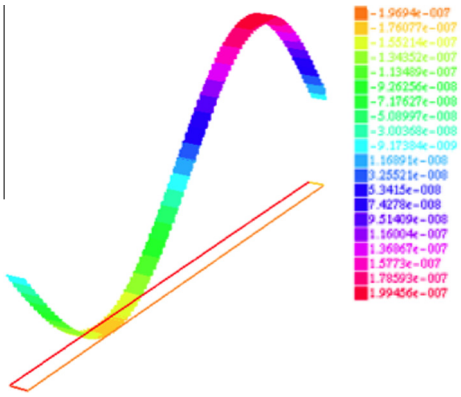

Fig. 10. Test 1: Iso-values final surface pressure (2D-model).

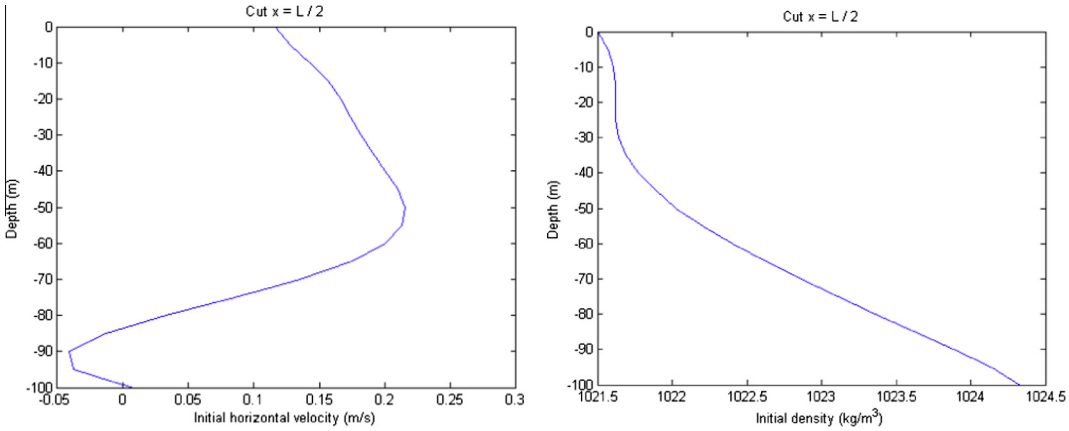

Fig. 11. Test 2: Initial horizontal velocity and density profiles (from left to right) at $x = L/2$.

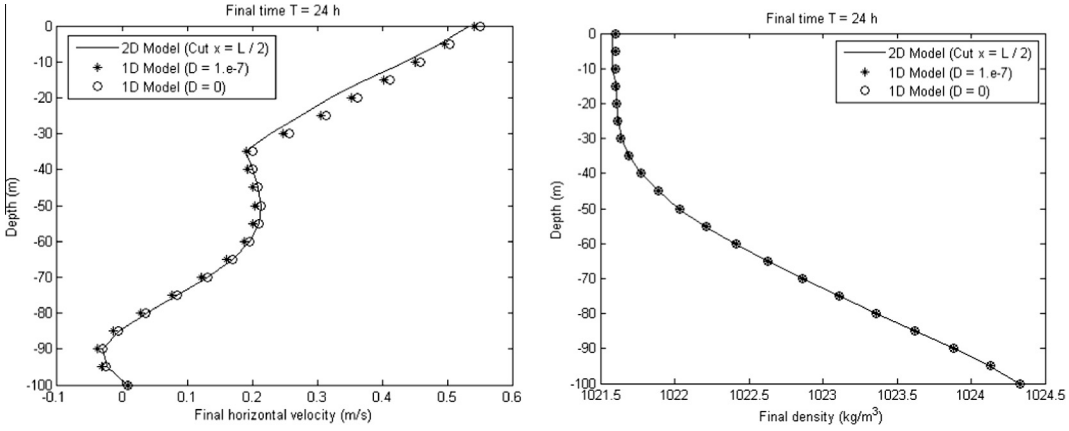

Fig. 12. Test 2: Comparison between 2D and 1D final horizontal velocity (left) and density (right).

Fig. 12 shows a comparison between the final horizontal velocity (on the left) and the final density (on the right) computed by the 2D model at $x = L/2$, and the 1D model (5) with the horizontal pressure gradient $D_u = D = 10^{-7}\ \mathrm{m}\cdot\mathrm{s}^{-2}$, and $D_u = D = 0\ \mathrm{m}\cdot\mathrm{s}^{-2}$.

From the final density profile we observe the formation of a mixed layer (almost constant density) of about 30 m depth, by using either the 2D model or the 1D model with a zero and non-zero pressure gradient D. A pycnocline is formed

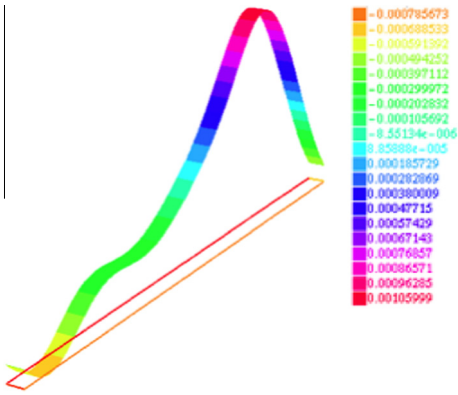

Fig. 13. Test 2: Iso-values final surface pressure (2D-model).

immediately below. This structure is quite similar to the one of the first test, where the initial density presented an unstable configuration.

Again in this test, the final fluid velocity and density obtained with the 2D model are horizontally homogeneous. Moreover, the vertical component of the velocity is almost zero. The final surface pressure, shown in Fig. 13, assumes its values in the range $[-1 \cdot 10^{-3}, 1 \cdot 10^{-3}]$.

The results of Fig. 12 stress that taking into account a non-zero horizontal pressure gradient in the 1D model does not improve the accuracy in the computation of the 2D mixing-layer profiles through the 1D mixing-layer model.

6. Conclusions

We have performed a non-linear stability analysis of algebraic turbulence models for oceanic mixing-layers. This analysis applies to negative (warming) surface thermodynamic fluxes, with bounded kinetic momentum from above and from below. In particular, it applies to tropical oceans in Earth.

We have obtained good stability properties for equilibria: The continuous perturbed model still present equilibria which are close to the equilibria of the un-perturbed model. The perturbed equilibria are unique and are asymptotically reached by time iterates of standard finite element discretizations. The numerical results show that the steady states for density are rather insensitive to perturbations, while those for zonal and meridional velocities are largely sensitive.

The unsteady flow is also stable under 2D perturbations. The 1D model provide mixing-layer profiles on time scales of the order of two days, which are accurate with respect to 2D perturbations of the initial conditions, and with respect to horizontal pressure gradients.

We finally conclude that algebraic turbulence models for oceanic mixing-layers bear excellent stability properties and provide good predictions of the formation of mixing-layer profiles and of flow equilibria, even with relatively large perturbations of the data.

Acknowledgment

Research partially supported by the Spanish Government Research Project MTM2009-07719.

References

[1] H. Burchard, K. Bolding, M.R. Villarreal, T.P. Rippeth, N. Fisher, A. Stips, The GOTM modelling system, in: H.Z. Baumert, J.H. Simpson, J. Sündermann (Eds.), Marine Turbulence: Theories Observations and Models, Cambridge University Press, Cambridge, 2005, pp. 213–224.
[2] Q. Wang, S. Danilov, J. Schröter, Finite Element Ocean circulation Model based on triangular prismatic elements, with application in studying the effect of topography representation, J. Geophys. Res. 113 (C05015) (2008), http://dx.doi.org/10.1029/2007JC004482.
[3] R.C. Pacanowski, S.G.H. Philander, Parametrization of vertical mixing in numerical models of the tropical oceans, J. Phys. Oceanogr. 11 (1981) 1443–1451.
[4] P.R. Gent, The heat budget of the toga-coare domain in an ocean model, J. Geophys. Res. 96 (1991) 3323–3330.
[5] A.C. Bennis, T. Chacón Rebollo, M. Gómez Mármol, R. Lewandowski, Numerical modelling of algebraic closure models of oceanic turbulent mixing layers, ESAIM: Math. Modell. Numer. Anal. 44 (2010) 1255–1277.
[6] Z. Kowalik, T.S. Murty, Numerical Modeling of Ocean Dynamics, World Scientific, 1993.
[7] T. Chacón Rebollo, M. Gómez Mármol, S. Rubino, On the existence and asymptotic stability of solutions for unsteady mixing-layer models, DCDS – A, J. Disc. Cont. Dyn. Syst. Ser. A 34 (2) (2014) 421–436.
[8] H. Brezis, Analyse Fonctionelle: Théorie et applications, Masson, 1983.
[9] E. Giusti, Minimal Surfaces and Functions of Bounded Variation, Birkhäuser, 1984.
[10] G.B. Folland, Real Analysis: Modern Techniques and their Applications, John Wiley & Sons, 1999.
[11] M. McPhaden, The tropical atmosphere ocean (tao) array is completed, Bull. Am. Meteorol. Soc. 76 (1995) 739–741.

[12] S. Rubino, Numerical modelling of oceanic turbulent mixing layers considering pressure gradient effects, MASCOT10, in: Proc.: IMACS Series in Comp. and Appl. Math., 16 (2011) 229–238.
[13] T. Chacón Rebollo, M. Gómez Mármol, S. Rubino, Numerical investigation of algebraic oceanic turbulent mixing-layer models, Nonlinear Processes Geophys. 20 (2013) 945–954.
[14] P. Delecluse, G. Madec, Oceanic modelling and the role of the ocean in the climate system, in: W.R. Holland, S. Joussaume, F. David (Eds.), Modeling the Earth's Climate and its Variability, Les Houches, Session LXVII 1997, Elsevier Science, 1999, pp. 237–313.
[15] J. Smagorinsky, General circulation experiment with the Primitive Equations I. The basic experiment, Mon. Weather Rev. 91 (3) (1963) 99–164.
[16] D.K. Lilly, The representation of small-scale turbulence in numerical simulation experiments, in: Proc. of the IBM Scientific Computing Symposium on Environmental Sciences, (1967) 195–210.
[17] T. Chacón Rebollo, F. Guillén González, An intrinsic analysis of existence of solutions for the hydrostatic approximation of Navier–Stokes equations, C.R. Acad. Sci. Paris, Ser. I 330 (2000) 841–846.
[18] F. Hecht, O. Pironneau, J. Morice, A. Le Hyaric, K. Ohtsuka, Freefem++ documentaion. Available on the web at: <http://www.freefem.org/ff++/>.
[19] R.E. Thomson, I.V. Fine, Estimating mixing layer depth from oceanic profile data, J. Atmos. Oceanic Technol. 20 (2) (2003) 319–329.